HHS Public Access

Author manuscript

Cancer Cell. Author manuscript; available in PMC 2018 October 09.

Published in final edited form as:

Cancer Cell. 2017 October 09; 32(4): 474–489.e6. doi:10.1016/j.ccell.2017.09.003.

Androgen Receptor Pathway-Independent Prostate Cancer Is Sustained through FGF Signaling

Eric G. Bluemn[1,2,9], **Ilsa M. Coleman**[2,9], **Jared M. Lucas**[2], **Roger T. Coleman**[2], **Susana Hernandez-Lopez**[2], **Robin Tharakan**[2], **Daniella Bianchi-Frias**[2], **Ruth F. Dumpit**[2], **Arja Kaipainen**[2], **Alexandra N. Corella**[2], **Yu Chi Yang**[2], **Michael D. Nyquist**[2], **Elahe Mostaghel**[1,2], **Andrew C. Hsieh**[1,2], **Xiaotun Zhang**[3], **Eva Corey**[3], **Lisha G. Brown**[3], **Holly M. Nguyen**[3], **Kenneth Pienta**[6], **Michael Ittmann**[7], **Michael Schweizer**[1], **Lawrence D. True**[4], **David Wise**[5], **Paul S. Rennie**[8], **Robert L. Vessella**[3], **Colm Morrissey**[3,*], and **Peter S. Nelson**[1,2,3,4,10,*]

[1]Department of Medicine, University of Washington, Seattle, WA, USA

[2]Divisions of Human Biology and Clinical Research, Fred Hutchinson Cancer Research Center, Mailstop D4-100, 1100 Fairview Avenue N, Seattle, WA 98109-1024, USA

[3]Department of Urology, University of Washington, 1959 NE Pacific Street, Seattle, WA 98195, USA

[4]Department of Pathology, University of Washington, Seattle, WA, USA

[5]Memorial Sloan-Kettering Cancer Center, New York, NY, USA

[6]Johns Hopkins University, Baltimore, MD, USA

[7]Baylor College of Medicine, Houston, TX, USA

[8]Vancouver Prostate Centre, Vancouver, BC, Canada

SUMMARY

Androgen receptor (AR) signaling is a distinctive feature of prostate carcinoma (PC) and represents the major therapeutic target for treating metastatic prostate cancer (mPC). Though highly effective, AR antagonism can produce tumors that bypass a functional requirement for AR, often through neuroendocrine (NE) transdifferentiation. Through the molecular assessment of mPCs over two decades, we find a phenotypic shift has occurred in mPC with the emergence of an AR-null NE-null phenotype. These “double-negative” PCs are notable for elevated FGF and MAPK pathway activity, which can bypass AR dependence. Pharmacological inhibitors of MAPK

[*]Correspondence: cmorriss@uw.edu (C.M.), pnelson@fhcrc.org (P.S.N.).
[9]These authors contributed equally
[10]Lead Contact

SUPPLEMENTAL INFORMATION

Supplemental Information includes seven figures and one table and can be found with this article online at http://dx.doi.org/10.1016/j.ccell.2017.09.003.

AUTHOR CONTRIBUTIONS

P.S.N., E.G.B., and C.M. conceived the project; E.G.B., S.H.-L., E.C., and H.M.N. performed mouse experiments; I.M.C., R.T.C., A.K., R.T., and D.W. performed sequencing and bioinformatics analyses; E.G.B., J.M.L., D.B.-F., R.F.D., A.N.C., Y.C.Y., M.D.N., and L.G.B. conducted molecular and cell biology experiments; X.Z., L.D.T., and M.I. provided pathology evaluation; E.M., A.H., M.S., K.P., R.L.V., and P.S.R. provided biospecimens, model systems, and clinical expertise; P.S.N., I.M.C., and C.M. wrote the manuscript; all authors reviewed and edited the manuscript.

or FGFR repressed the growth of double-negative PCs *in vitro* and *in vivo*. Our results indicate that FGF/MAPK blockade may be particularly efficacious against mPCs with an AR-null phenotype.

INTRODUCTION

Androgen deprivation therapy (ADT), achieved through surgical or pharmacological approaches, exploits the exquisite dependence of prostate carcinoma (PC) on androgen receptor (AR) signaling. Although initially highly effective as a treatment for metastatic PC, ADT is characterized by the predictable emergence of resistance, a disease state termed castration-resistant prostate cancer (CRPC). An important feature of CRPC is the reactivation of AR signaling, an event reflected by progressive rises in serum prostate-specific antigen (PSA), a gene product transcriptionally regulated by the AR. A substantial body of evidence has documented that essentially the entire AR cistrome is re-expressed in most CRPCs, and several mechanisms capable of maintaining AR activity have been established (Carver et al., 2011; Montgomery et al., 2008; Nelson et al., 2002; Taylor et al., 2010).

The continued importance of AR signaling in most advanced PCs has prompted the development of therapeutics directed toward further suppressing AR ligands or the AR itself. Several drugs, including improved AR antagonists and inhibitors of androgen synthesis, extend survival (de Bono et al., 2011; Scher et al., 2012), although to date complete remissions have been rare. While the intensive effort focused on completely repressing AR activity may completely eradicate a subset of PCs, this selective pressure has the potential to generate PCs reliant on survival mechanisms distinct from those regulated by AR or that substitute for vital AR functions.

Assessments of metastatic CRPCs have determined that patients may harbor tumor deposits that do not express AR following conventional ADT (Roudier et al., 2003; Shah et al., 2004). While a subset of AR-null tumors express markers of neuroendocrine (NE) differentiation, these neuroendocrine prostate cancers (NEPC) exist within a more complex spectrum of phenotypes ranging from anaplastic carcinomas, mixed prostatic adenocarcinomas with NE features, to pure small-cell carcinomas (Aparicio et al., 2011; Beltran et al., 2011; Tzelepi et al., 2012). Importantly, there are metastatic CRPCs that do not express the AR or markers of NE differentiation (Roudier et al., 2003; Wang and Epstein, 2008). Although conclusive data are lacking, evidence suggests that the widespread application of more effective AR pathway antagonists such as enzalutamide (ENZ) and abiraterone (ABI) is shifting the pattern of metastasis in patients with CRPC accompanied by alterations in their molecular landscapes (Beltran et al., 2014; Doctor et al., 2014). Anticipating that effective AR repression will more routinely result in CRPCs devoid of AR signaling, we sought to identify molecular pathways operating in CRPC that function to promote survival and growth in the absence of AR activity. The emergent signaling programs that confer resistance to AR-directed therapeutics may represent treatment targets for men with progressive CRPC.

RESULTS

Emergence of an AR-Null and Neuroendocrine-Null Prostate Cancer Phenotype in Patients Following AR-Directed Therapy

To evaluate the shifting phenotypic and molecular landscapes of metastatic CRPC (mCRPC), we characterized metastatic tumors acquired from a long-standing tissue acquisition necropsy program spanning two decades. We classified tumors from 84 consecutive patients as androgen receptor pathway active prostate cancer (ARPC) if they expressed AR and the AR-regulated gene PSA, or NEPC if they expressed the NE gene synaptophysin (SYP). In a small minority of patients both ARPC and NEPC tumors were evident. In the era prior to the approval of the AR pathway antagonists ENZ and ABI (1997–2011), most CRPCs were ARPCs (85%) with rare NEPCs (10%) and rarer AR^{-}/NE^{-} tumors (5%), hereafter classified as “double-negative” PCs (DNPC) (Figures 1A and 1B). In the contemporary era (2012–2016), we observed a shift in tumor phenotypes with a higher representation of DNPCs (Figure 1 A). Gene expression programs of the tumors classified by immunohistochemistry (IHC) supported these distinct subtypes using 10-gene signatures that were concordant with previously published gene sets indicative of NE and AR pathway activity (Figures 1C, S1A, and S1B) (Beltran et al., 2016; Hieronymus et al., 2006).

While molecular characteristics of CRPCs with active AR and NE programs are well described, those of DNPC are not established. We used RNA sequencing (RNA-seq) to quantitate gene expression differences between DNPCs and ARPCs and identified 417 and 107 mRNAs with substantially increased or decreased levels, respectively (5-fold; $q < 0.0001$) (Figure 1D). In comparison with NEPC, 162 and 594 genes were significantly increased or decreased, respectively in DNPCs (5-fold; $q < 0.0001$) (Figure S1C). Gene set enrichment analysis (GSEA) identified numerous biological processes that differed between ARPC and DNPC, which complicated efforts to identify a predominant driver event or signaling pathway (Figure S1D). To prioritize efforts defining causal mechanisms underlying DNPC, we evaluated tumors for genomic alterations and partitioned mCRPCs that we previously characterized for genome-wide copy-number and mutation status (Kumar et al., 2016) into categories of ARPC, NEPC, and DNPC based on their expression profiles (Figures 1E, 1F, S1E, and S1F). Common aberrations in CRPCs such as *TP53* mutation and *PTEN* loss did not differ significantly across groups with the exception of *AR* amplification, which was more frequent in ARPC (66%) compared with NEPC (13%) ($p = 5.6 \times 10^{-5}$) and *RB1* loss, a hallmark of NEPC, which differed between NEPC (88%) and ARPC (16%) ($p = 2.4 \times 10^{-8}$) (Figure 1E). Several genomic regions differed in copy number between ARPC and DNPC, but no genes in these regions varied in expression by more than 2-fold (Figure 1F). With the caveat of limited tumor numbers, these data indicate that recurrent genomic aberrations do not underlie the marked phenotypic differences between ARPC and DNPC.

AR Ablation Results in CRPC without Neuroendocrine Differentiation

To provide insights into causal mechanisms capable of promoting survival in an AR-null state, we developed a model system that recapitulated the transition from a tumor initially dependent on AR activity to one capable of AR-independent growth. We began with the LNCaP cell line, a widely studied androgen-sensitive *in vitro* model of PC. LNCaP

derivatives capable of proliferating in the absence of AR ligands typically continue to exhibit AR signaling (Sobel and Sadar, 2005). Furthermore, targeting the AR in these cells with antibodies, ribozymes, or RNAi induces apoptosis or growth arrest, indicating that the AR maintains vital functions (Cheng et al., 2006; Zegarra-Moro et al., 2002). To initiate the present studies, we used a LNCaP line stably transduced with a tetracycline (TET)-inducible anti-AR short hairpin RNA (shRNA) (Cheng et al., 2006), designated as LNCaP^{shAR}. Repressing AR in the setting of castration-resistant LNCaP^{shAR} growth results in tumor regression, but recurrent LNCaP^{shAR} tumors re-express AR, due to the selective loss or silencing of the AR-directed shRNA (Snoek et al., 2009). To enforce AR ablation, we introduced an androgen response element (ARE)-driven thymidine kinase suicide gene designated pATK. In the resulting LNCaP$^{shAR/pATK}$ line, thymidine kinase is expressed in the setting of an active AR and induces cell death when treated with ganciclovir (Figures 2A and S2A–S2C).

We subjected LNCaP$^{shAR/pATK}$ cells to increasingly severe AR pathway suppression (Figure 2A). After 2 weeks of androgen deprivation (ADT), medium was supplemented with 1 μg/mL doxycycline (Dox) to induce the anti-AR shRNA, which produced >99% cell death. After 5 months, a residual population of viable cells remained. This colony was treated with a 2-week course of ganciclovir to eliminate cells expressing functional AR. Surviving cells were designated LNCaP-AR Program-Independent Prostate Cancer (LNCaP^{APIPC}). AR and PSA were nearly undetectable in LNCaP^{APIPC}: AR expression was 45-fold lower and PSA expression was 30-fold lower than LNCaP$^{shAR/pATK}$ (Figures 2B and 2C). Transcripts comprising an AR activity signature were all substantially decreased in LNCaP^{APIPC} cells and showed no induction with androgen treatment (Figure 2D). We confirmed the absence of AR and PSA protein expression in LNCaP^{APIPC} grown *in vivo* as subcutaneous xenografts (Figure 2E).

Previous studies demonstrated that LNCaP cells grown in androgen-depleted medium or with AR antagonists display a transdifferentiated phenotype resembling NEPC (Mu et al., 2017; Zhang et al., 2003). NEPC is characterized by loss of AR expression and AR activity and increased expression of CHGA and SYP, and cells often exhibit small-cell morphology (Beltran et al., 2011). NE-associated genes were not upregulated in LNCaP^{APIPC} cells grown with or without androgen supplementation (Figure 2F). Furthermore, LNCaP$^{shAR/pATK}$ and LNCaP^{APIPC} grown as murine xenografts do not express CHGA or SYP protein (Figure 2E).

To further evaluate the characteristics of LNCaP^{APIPC} cells, we determined the effects of AR pathway-targeted therapies. In contrast to parental LNCaP$^{shAR/pATK}$, LNCaP^{APIPC} grow robustly without androgen (Figure 2G). Furthermore, treatment of LNCaP$^{shAR/pATK}$ with ENZ completely inhibited growth, while LNCaP^{APIPC} was highly resistant to ENZ treatment (Figure 2G). PC cells with low AR transcriptional activity that accompanies advanced Gleason grade exhibit invasive and metastatic pheno-types (Aihara et al., 1994; Erbersdobler et al., 2009). LNCaP^{APIPC} cells displayed a slight but consistent increase in baseline migration (5%, $p = 0.019$) and invasion (12%, $p = 0.006$) when compared with LNCaP$^{shAR/pATK}$, and also responded to a trans-well serum gradient with a higher number of migratory and invasive cells (Figures 2H and 2I).

FGFR and MAPK Signaling Pathways Are Activated in Androgen Receptor Pathway-Independent Prostate Cancer

The growth of LNCaP^{APIPC} cells in the absence of AR expression indicated that alternative survival pathways supplanted AR requirements and we next sought to identify them. We used RNA-seq to profile the gene expression program in LNCaP^{APIPC} and identified 548 differentially expressed transcripts relative to AR-intact LNCaP$^{shAR/pATK}$ cells (≥10-fold; q<0.001) (Figure 3A). LNCaP^{APIPC} gained expression of basal cell genes such as *TP63* and *TRIM29*, and retained expression genes expressed in luminal cells such as *KRT8*, *KRT18*, and *HPN* (Figure 3B). We used array CGH to identify copy-number aberrations harboring genes that could bypass a requirement for AR signaling. Overall, the genomes of LNCaP^{APIPC} and parental LNCaP$^{shAR/pATK}$ were nearly identical, with only seven regions differing in copy number between the two lines. Two genes, *MAT2B* and *KIAA1328*, exhibited concordant changes in copy number and expression, but transcript levels did not differ between ARPCs and DNPCs. Though located in the region of chromosome-3 copy gain, *WNT7A* transcripts were not measureable in LNCaP^{APIPC} cells (Figures S3A–S3C). Collectively, the few genomic aberrations identified do not explain the marked alterations in gene expression between LNCaP^{APIPC} and parental LNCaP$^{shAR/pATK}$ cells.

To confirm lineage relationships, we compared the expression profiles of 15 PC cell lines with LNCaP^{APIPC} using unsupervised hierarchical clustering. LNCaP^{APIPC} grouped with other LNCaP derivatives, indicating that LNCaP^{APIPC} retains LNCaP characteristics even while lacking AR-regulated gene expression (Figure 3C). Notably, the removal of Dox from the culture medium of LNCaP^{APIPC} cells did not result in AR re-expression or a reversion of gene expression changes (Figure S4A). We also found no evidence of upregulation of the glucocorticoid receptor (*GR/NR3C1*), a nuclear hormone receptor previously shown to bypass AR requirements (Arora et al., 2013) (Figure 3D).

Phosphatidylinositol 3-kinase (PI3K)/AKT signaling can influence the progression of CRPC and effectively compensate for reduced AR activity in PC models via reciprocal feedback activation (Carver et al., 2011; Mulholland et al., 2011). Therefore, we hypothesized that PI3K pathway upregulation was supporting LNCaP^{APIPC} growth. Consistent with previous studies, pAKT levels increased in AR-intact LNCaP$^{shAR/pATK}$ cells grown in androgen-depleted medium (Figure 3E). Surprisingly, pAKT was nearly undetectable in LNCaP^{APIPC}, suggesting that PI3K activity is not acting as a survival/growth pathway in these AR-null cells.

Increased mitogen-activated protein kinase (MAPK) signaling is also postulated to support CRPC proliferation (Aytes et al., 2013; Mulholland et al., 2012; Ueda et al., 2002). MAPK signal transduction is activated through a variety of stimuli, and is closely associated with receptor tyrosine kinase (RTK) activity. Phosphorylated MEK and dually phosphorylated ERK1/2 (ppERK1/2) were elevated in LNCaP^{APIPC} compared with LNCaP$^{shAR/pATK}$ (Figure 3F). These data suggested that increased MAPK signaling may be sustaining AR-independent growth in LNCaP^{APIPC}. We evaluated *RAS* and *RAF* for alterations that could account for MAPK activation but found no evidence of altered expression or functional mutations (Figures S4B and S4C).

We next evaluated the LNCaP^{APIPC} transcriptome for mechanisms plausibly contributing to MAPK activity and found that *fibroblast growth factor 8* (*FGF8*) expression was substantially upregulated relative to AR-active LNCaP$^{shAR/pATK}$ (>100-fold, $q < 0.001$) (Figure 3G). *FGF8* is transcribed as eight distinct isoforms (FGF8a–h), and of these FGF8b has the most oncogenic effects (MacArthur et al., 1995). LNCaP^{APIPC} expressed all active FGF8 isoforms at substantially higher levels than LNCaP$^{shAR/pATK}$ (FGF8a/g = 1,100-fold, $p < 0.001$; FGF8b = 600-fold, $p < 0.001$) (Figures 3H and 3I). FGF8 protein was detected in serum-free conditioned medium from LNCaP^{APIPC} but not from LNCaP$^{shAR/pATK}$, concordant with transcript expression results (Figures 3J and S4D).

To further assess FGF pathway activity, we measured a panel of transcripts shown to reflect the dynamic output of FGF receptor (FGFR) signaling (Delpuech et al., 2016). Several transcripts comprising this FGFR signature were increased more than 10-fold in LNCaP^{APIPC} cells including *DUSP6*, *ETV4*, and *EGR1*, and LNCaP^{APIPC} cells showed significant FGFR and MAPK pathway enrichment scores (Figure 3K). FGF pathway activation has been shown to occur in rare instances by FGFR genomic rearrangements in mCRPC (Wu et al., 2013), but we found no evidence of mutation, copy-number gain, or gene rearrangements involving *FGF8* or FGFRs in LNCaP^{APIPC} (Figures S3B and S3C). Collectively, these data supported the hypothesis that an autocrine FGF signaling program is activated in LNCaP^{APIPC} in the absence of AR to maintain cell survival and growth via MAPK.

FGFR and MAPK Signaling Are Active in DNPC and Are Inversely Associated with AR Activity

We next sought to further evaluate FGF and MAPK signaling in DNPCs and confirm LNCaP^{APIPC} as a relevant model for this CRPC subtype. We determined that an LNCaP^{APIPC} gene signature is significantly enriched in DNPC metastases (false discovery rate [FDR] < 0.001) (Figure 4A), as are gene sets reflecting the activity of FGF signaling, MAPK activity, MEK/ERK, and EMT (Figure 4B). No single FGF ligand or receptor was universally increased across all DNPCs: individual tumors expressed high *FGF1*, *FGF8*, or *FGF9*, and different FGFRs. Each of these secreted FGF ligands has been shown to activate multiple FGFRs consistent with the finding that DNPCs exhibited consistently high MEK/ERK and FGF activity scores (Figures 4C and 4D). A small subset of ARPCs also expressed high MEK/ERK and FGFR pathway activity, and these tumors generally also had lower AR activity (Figure 4C). Across the full spectrum of CRPC metastases, AR activity was inversely associated with FGF8/9 expression, and FGFR activity (e.g., $r = -0.48$, $p < 0.001$ for FGF8) (Figure 4E). AR and FGF8/9 expression were inversely associated ($r = -0.13$) in an independent dataset of 150 metastatic CRPC tumors from the SU2C/PCF dataset (data not shown) (Robinson et al., 2015). Collectively, these results couple elevated FGF and MAPK signaling with a CRPC tumor phenotype, DNPC, which lacks AR activity and supports LNCaP^{APIPC} as a model that represents these attributes of DNPC.

To address the challenge of deriving a generalized understanding of DNPC from a single model, we sought to develop additional systems with which to evaluate drivers of DNPC and identify effective therapeutics. As with LNCaP^{APIPC}, our objective was to begin with an

AR-positive PC and then repress AR activity. We were unable to successfully eliminate AR in the commonly used VCaP or 22Rv1 PC lines by shRNA or CRISPR-based approaches (data not shown). However, using the PacMet-UT1 PC line that expresses a functional AR (Troyer et al., 2008), albeit with attenuated activity, we were able to excise AR using CRISPR/Cas9 editing and generate multiple PacMet AR-null sublines (Figures 5A and 5B). AR loss was associated with 10-fold upregulation of *FGF9* and enhancement of FGF and MAPK activity (Figures 5C and 5D). Notably, repressing AR activity in PacMet-UT1 cells did not result in an NEPC phenotype, and the expression of *SOX2*, a reprogramming factor associated with transdifferentiation to NEPC, was decreased (Figure 5C) (Mu et al., 2017).

We were also successful in generating a patient-derived xenograft (PDX) model of DNPC, designated LuCaP173.2, initiated from a tumor acquired from a rapid autopsy procedure. Metastatic tumors from this individual had phenotypic variability, with one rib metastasis expressing AR and PSA and a second rib metastasis lacking AR or PSA staining (Figure 5E). We confirmed that the LuCaP173.2 PDX lacks AR and PSA expression and does not express classic NE markers such as chromogranin or synaptophysin, thus fulfilling criteria for DNPC (Figure 5F). However, other genes associated with an NE phenotype such as *EZH2* and *MYCN* are expressed in this PDX line, suggesting a continuum of tumor differentiation (Figure S5). In accord with findings in DNPC metastases, LuCaP173.2 expresses high *FGF9* and *FGFR1* levels with low AR and NEPC program scores and a high FGFR activity score (Figure 5G).

FGF Activates MAPK Signaling and Bypasses a Requirement for Androgens and the AR in Promoting Prostate Cancer Growth

We next sought to determine whether FGF signaling is necessary and sufficient for bypassing a requirement for AR activity. We hypothesized that the substantial upregulation of FGF8 in LNCaP^{APIPC} cells comprises an autocrine loop to sustain cell survival in the absence of AR. The introduction of FGF8-specific small interfering RNAs (siRNAs) reduced LNCaP^{APIPC} growth by 80% ($p < 0.001$) (Figure 6A). In contrast, siRNA knockdown of FGF9, which is not upregulated in LNCaP^{APIPC}, had no effect. Exogenous FGF8b increased the growth of parental LNCaP$^{shAR/pATK}$ in androgen-depleted conditions ($p < 0.001$) and the addition of concentrated LNCaP^{APIPC} conditioned medium (CM) showed a small but statistically significant increase in proliferation (11%, $p = 0.01$), whereas LNCaP$^{shAR/pATK}$ CM had no effect (Figure 6B). The addition of exogenous FGF8b increased ERK1/2 phosphorylation in both LNCaP$^{shAR/pATK}$ and LNCaP^{APIPC}. FGF8-induced growth in androgen-depleted conditions and ERK1/2 phosphorylation were blocked by treatment with the FGFR inhibitor PD173074 (Mohammadi et al., 1998) (Figures 6C and 6D).

To demonstrate that FGF8 was sufficient to promote the growth of cells cultured under total AR pathway suppression, we treated parental LNCaP$^{shAR/pATK}$ grown in androgen-deprived conditions with Dox to suppress AR expression, and added FGF8b. FGF8b maintained cell proliferation during AR pathway ablation (30% increase in cell number compared with untreated LNCaP$^{shAR/pATK}$; $p = 0.019$), albeit at a lower rate than AR-intact LNCaP$^{shAR/pATK}$ (75% increase in cell number compared with untreated LNCaP$^{shAR/pATK}$;

p = 0.018) (Figure 6E). In a parallel experiment, LNCaP$^{shAR/pATK}$ cells were cultured in androgen-depleted medium and AR expression was suppressed by pre-treatment with Dox for 72 hr. Addition of exogenous FGF8b rescued the growth inhibition by ADT and AR suppression (58% increase in growth compared with untreated LNCaP$^{shAR/pATK}$; p = 0.003) (Figure S6A).

The FGFR antagonist PD173074 is a nanomolar inhibitor of FGFR1 but is also a submicromolar inhibitor of vascular endothelial growth factor receptor 2/kinase domain receptor (VEGFR2/KDR) (Mohammadi et al., 1998). To confirm that FGFR antagonism is mediating the growth repression in DNPC, we treated LNCaP^{APIPC} with a second FGFR antagonist CH-5183284, which potently and selectively inhibits FGFR1–3 (IC_{50} of 8–22 nM) without significant biological effects toward VEGFR2/KDR or other kinases (Nakanishi et al., 2014). At concentrations of 0.1–1.0 μM, CH-5183281 substantially inhibited the viability and increased apoptosis rates in LNCaP^{APIPC} with effects far exceeding those observed in wild-type LNCaP cells (Figures 6F and 6G). CH-5183281 also reduced the viability of AR-null PacMet-UT1 cells relative to the AR-intact parental line (Figure 6H). Confirming that MAPK activity is required for FGF8-mediated castration-resistant proliferation, the MEK1/2 inhibitor U0126 blocked the growth of LNCaP$^{shAR/pATK}$ induced by FGF8 in androgen-depleted conditions (p < 0.001; Figure 6I) and repressed LNCaP^{APIPC} proliferation. Co-treatment of a second androgen-sensitive PC line, 22RV1, with U0126 and FGF8 led to a 46% decrease in cell number compared with cells treated with FGF8 alone (p < 0.001; Figure S6B).

We next sought to determine whether suppressing FGF signaling would inhibit the growth of DNPC *in vivo*. PD173074 significantly reduced LNCaP^{APIPC} xenograft growth rates: the study was terminated at 40 days due to large tumors in the control group at which time tumor volumes were 1,147 mm^3 in the vehicle and 571 mm^3 in PD173074 arms (p < 0.001) (Figure 6J). To confirm these findings, we treated LuCaP173.2 DNPC PDX tumors with CH-5183284. At the study endpoint of 24 days, tumor volumes were 814 mm^3 and 170 mm^3 in the vehicle and CH-5183284 arms, respectively (p < 0.001) (Figure 6K). The expression of FGFR pathway genes as well as composite FGFR and MEK/ERK pathway activity were significantly reduced in LuCaP173.2 tumors resected 3 days and 24 days on CH-5183284 treatment (Figure 6L).

FGF- and MAPK-Induced ID1 Contributes to AR-Null Prostate Cancer Growth

We next evaluated LNCaP^{APIPC} for downstream mediators of FGF/MAPK signaling that could promote the dedifferentiated phenotype of DNPC and support survival in the absence of AR activity. We identified a strong candidate for this role, *inhibitor of differentiation 1* (*ID1*), which was upregulated in LNCaP^{APIPC} compared with LNCaP$^{shAR/pATK}$ (~10-fold by RNA-seq; q < 0.001; 5-fold byqRT-PCR) (Figure 7A). ID1 expression is induced by exogenous FGF and bone morphogenetic protein via MAPK pathway activation (Langenfeld and Langenfeld, 2004; Passiatore et al., 2011), prevents differentiation by binding cell lineage-specific transcription factors (Perk et al., 2005), and has been associated with poorly differentiated PC (Coppe et al., 2004; Sharma et al., 2012). Notably, other ID family members were also increased in LNCaP^{APIPC} and the LuCaP173.2 DNPC PDX (Figure 7B).

ID1 levels are significantly higher in DNPC metastases relative to ARPCs ($p < 0.005$) (Figure 7C), and ID1 and AR expression are inversely associated in mCRPC (Pearson correlation = −0.39) (Figure 7D).

Stimulation of LNCaP$^{shAR/pATK}$ cells with FGF8 resulted in a 4-fold ($p = 0.006$) increase in ID1 mRNA and protein (Figures 7E and 7F). MEK inhibition reduced FGF8-mediated *ID1* induction by approximately 30% ($p = 0.005$) (Figure 7E). Although ID1 levels were already elevated, stimulation of LNCaP^{APIPC} with exogenous FGF8 resulted in a further 1.6-fold increase ($p < 0.001$), and treatment with U0126 alone decreased baseline *ID1* expression by approximately 40% ($p = 0.006$) (Figure 7E). We also observed a significant upregulation of ID1 in response to FGF8 treatment in androgen-sensitive 22Rv1 cells (Figures S7A and S7B). The enhanced activity of specific RTKs is associated with ligand-independent activation of AR transcription in some models (Gregory et al., 2005; Yang et al., 2003); however, we did not observe a change in *AR, PSA*, or *TMPRSS2* expression in response to FGF8b stimulation in androgen-deprived LNCaP$^{shAR/pATK}$, LNCaP^{APIPC}, or 22Rv1 cells (Figures 7G and S7C).

ID1 has been shown to influence PC differentiation and proliferation (Ling et al., 2011; Ouyang et al., 2002), and we hypothesized that ID1 could mediate a component of the growth-promoting effects of FGF/MAPK activity. In support of this hypothesis, levels of ID1–3 transcripts were diminished in the LuCaP173.2 DNPC PDX tumors treated with the FGFR inhibitor CH-5183284 (Figure 7H). ID1 knockdown did not significantly affect LNCaP$^{shAR/pATK}$ growth compared with a scrambled control siRNA (siUNI). In contrast, two independent ID1-targeting siRNAs decreased LNCaP^{APIPC} growth by 32% ($p = 0.003$) and 43% ($p < 0.001$) (Figure 7I). When LNCaP$^{shAR/pATK}$ were treated with FGF8, ID1 knockdown significantly attenuated FGF8-induced proliferation by ~35% ($p < 0.001$). The effect of ID1 knockdown was enhanced in LNCaP^{APIPC} with ID1 siRNAs suppressing FGF8-induced growth by 39%-50% ($p < 0.001$) (Figure 7I). These effects were replicated in 22RV1 cells grown in androgen-deprived conditions (Figure S7D).

DISCUSSION

Therapeutic approaches designed to impair AR activity remain first-line therapy for men with metastatic PC. While resistance to AR-directed therapeutics is usually accompanied by reactivation of AR signaling, newer drugs with potent AR pathway antagonism appear to be shifting the phenotypes of resistant PC to anaplastic and NE carcinomas that are devoid of AR activity (Figure 7J). The AR-null/NE-null tumors evaluated in the present study were acquired from men after initial responses to AR antagonists, indicating that these agents effectively eliminated tumor clones dependent on the AR, but failed to eradicate cell populations that no longer required AR signaling. Defining the drivers of these resistant carcinomas is critical for the development of effective treatment strategies.

We determined that complete AR pathway independence was associated with elevated autocrine FGF signaling *in vitro* and elevated FGFR and MAPK pathway activity in mCRPC. FGF ligands and receptors have previously been shown to influence the development and progression of PC (Acevedo et al., 2007; Feng et al., 2015). Of relevance

to the present study, a PDX model of PC devoid of AR signaling was shown to express high levels of FGF9, which promoted tumor growth, induced an osteoblastic tumor microenvironment, and responded to FGF-directed therapy (Li et al., 2008). MAPK signaling promotes poorly differentiated tumor growth in models of PC (Mulholland et al., 2012), and constitutive ERK1/2 activity is associated with castration resistance (Gioeli et al., 1999; Oka et al., 2005; Rodriguez-Berriguete et al., 2012). While there is evidence suggesting that MAPK can stimulate ligand-independent AR activity (Feldman and Feldman, 2001), FGF/MAPK signaling did not promote the re-expression of AR-regulated genes in our models and FGFR activity was inversely associated with the expression and activity of AR in CRPCs. At this time, the mechanism(s) influencing FGF expression in $LNCaP^{APIPC}$ or other DNPCs is not known. As we found no recurrent genomic events involving FGFs/FGFRs, other processes capable of influencing FGF transcription, including epigenetic regulation, are likely operative. Notably, a small subset of CRPCs exhibiting FGFR/MAPK activity did not express high levels of FGF ligands, suggesting that in some circumstances paracrine FGF derived from microenvironment constituents may promote pathway activity and drive treatment resistance (Lawson et al., 2010).

While AR repression can allow for cellular reprogramming and transdifferentiation to NE carcinoma (Ku et al., 2017; Zou et al., 2017), our results indicate that the acquisition of NE characteristics may represent a continuum of differentiation from ARPC to DNPC to NEPC, although the acquisition of NE characteristics does not appear to be a certainty following AR ablation (Figure 7J). Importantly, alternative cell fates may associate with unique therapeutic vulnerabilities. Given that NE and anaplastic tumors are more common following sustained AR pathway suppression and appear to arise from adenocarcinomas *in vivo* based on shared genomic aberrations (Beltran et al., 2011, 2016), it is quite likely that the incidence of AR pathway-independent PCs will increase with the deployment of increasingly potent AR inhibition. Whether acute and more complete AR repression will eliminate PCs or consistently generate AR-null variants remains to be determined. Early results from an ongoing clinical trial (NCT00831792) of the FGFR antagonist dovitinib in men with metastatic CRPC unselected for loss of AR activity reported a 26% response rate in bone and soft tissue lesions (Wan et al., 2014). Our results suggest that FGFR inhibition may have modest effects in AR-active CRPCs, but be particularly active in the subset of CRPCs with absent or limited AR function. A clinical trial of FGFR or MAPK antagonists may be fruitful in patients stratified by AR activity status. Furthermore, co-targeting of predictable AR bypass pathways capable of providing robust cell survival and proliferation signals may prolong responses to initial AR antagonism.

STAR★METHODS

Detailed methods are provided in the online version of this paper and include the following:

- KEY RESOURCES TABLE
- LEAD CONTACT FOR REAGENT AND RESOURCE SHARING
- EXPERIMENTAL MODELS AND SUBJECT DETAILS
  - Cell Lines

STAR★METHODS

LEAD CONTACT FOR REAGENT AND RESOURCE SHARING

For further information and requests for reagents may be directed to and will be fulfilled by the corresponding author Peter S. Nelson (pnelson@fredhutch.org).

EXPERIMENTAL MODELS AND SUBJECT DETAILS

Cell Lines—All cells were maintained at 37°C in a 5% CO_2 incubator. LNCaP (ATCC), 22RV1 (ATCC), and PacMet-UT1 (gift of D.A. Troyer) prostate cancer cell lines were grown in RPMI1640 (Invitrogen) supplemented with 10% FBS (Invitrogen) and 1% PenStrep (Invitrogen). NCI-H660 (ATCC) cells were grown in RPMI 1640 supplemented with 0.005 mg/ml insulin, 0.01 mg/mL transferrin, 30 nM sodium selenite, 10 nM hydrocortisone, 10 nM beta-estradiol, 4 mM L-glutamine, 5% FBS and 1% PenStrep. LNCaP^{shAR} (gift of P.S. Rennie) were grown in RPMI1640 + 5%FBS +1% PenStrep + 2.5 μg/mL Blasticidin (Invitrogen) + 1 μg/ml Puromycin (Invitrogen). LNCaP$^{shAR/pATK}$ (this study) were maintained in RPMI1640 + 5% FBS +1% PenStrep + 2.5 μg/mL blasticidin + 1 μg/ml puromycin + 25 μg/ml Zeocin (Invitrogen). LNCAP^{APIPC} (this study) were maintained in RPMI1640 + 5% CSS (Charcoal Dextran stripped FBS) (Gemini) + 1 % PenStrep + 2.5 μg/mL blasticidin + 1 μg/ml puromycin + 25 μg/ml Zeocin + 1 μg/mL doxycycline (Clontech). Cell lines were authenticated by STR analysis by DDC Medical (Fairfield, OH).

Tissue Acquisition—Samples were obtained from male patients who died of metastatic CRPC and who signed written informed consent for a rapid autopsy performed within 8 hours of death, under the aegis of the Prostate Cancer Donor Program at the University of Washington. The Institutional Review Boards of the University of Washington and of the Fred Hutchinson Cancer Research Center approved this study. LuCaP xenograft lines were established from specimens acquired at either radical prostatectomy or at autopsy, implanted, and maintained by serial passage in intact immune compromised male mice.

CRPC was assessed using immunohistochemical analysis to determine the distribution of adenocarcinoma (AR^+), double-negative (AR^-/NE^-), and neuroendocrine (AR^-/NE^+) in these metastasis. Sites of metastases were ascribed a score between 0–200 for AR and SYP positivity. Any score <20 was categorized as negative to categorize each site.

LNCaP^{APIPC} Xenograft Mouse Models—NOD-scid IL2Rgamma^{null} mice were purchased from the FHCRC animal facility. LNCaP^{APIPC} cells were resuspended 1:1 in Matrigel (BD Biosciences) to a final concentration of 5×10^6 cells/ml and 100 μl of cells were injected subcutaneously into the flank of castrated male mice. Xenografts were measured with digital calipers every 2 days and tumor volume was calculated using the formula (π/6)(LxW2), where L is the length of the tumor and W its width. Animals implanted with LNCaP^{APIPC} xenografts were maintained on a diet supplemented with doxycycline (200 mg/Kg, Harlan). When tumors reached a total volume of 200 mm^3 animals were enrolled into treatment arms consisting of PD173074 given at 50 mg/Kg/day by oral gavage five times per week or control vehicle 99% PBS with 1% DMSO used to dissolve PD173074. Each treatment group was composed of 8 animals. Animals were sacrificed when tumors reached a volume of 1500 mm^3. All xenografts experiments were approved by the Fred Hutchinson Institutional Animal Care and Use Committee (File#1671).

PDX Mouse Models—The LuCaP 173.2 patient-derived xenograft (PDX) line is from a rib metastasis obtained at time of death from a patient with CRPC and implanted into 6 week old immunocompromised male mice. CB-17 SCID mice (Charles River) were implanted subcutaneously with LuCaP 173.2 tumor tissue. Animals underwent rolling enrollment once tumors reached 100 mm^3 and were randomized into one of two groups (Control vs. Treatment). The FGFR inhibitor CH5183284 (Debio-1347) (Selleck chem) was dissolved in 100% DMSO and a 10-fold concentration of dosing solution was prepared. Then an equal volume of Cremophor EL was added to DMSO solution (5-fold concentration of dosing solution in 50 vol% DMSO/50 vol% Cr-EL). This solution was divided into daily usage amounts and stored at 4°C until each dosing day. For dosing, the stock solution was diluted with diluent (18.8 vol% PEG400 / 18.8% HPCD in distilled water) by 5-fold concentration on each day. The final concentration of vehicle was 10 vol% DMSO/10 vol% Cr-EL/15 vol% PEG 400/15% HPCD in distilled water as per Nakanishi et al., 2014. LuCaP 173.2 tumor bearing animals received either vehicle (Control), while treated animals (Treatment) received 80 mg/kg CH5183284 4 days a week for 3.5 weeks via oral gavage. Note, 6 animals in the treated group received 100 mg/kg CH5183284 for 5 days/daily for one week before switching over to 80 mg/kg CH5183284 4 days a week due to loss of body weight. Tumor volumes (TV) were measured using digital calipers (calculated as (π/6)

(LxW2)) and body weights (BW) were measured twice weekly. Animals were euthanized after 3.5 weeks, when tumors exceeded 1,000 mm^3, or when animals became otherwise compromised. The tumors were then divided equally into paraffin blocks with the remainder flash frozen for subsequent sequencing analysis. All PDX experiments were approved by the University of Washington Institutional Animal Care and Use Committee (File #2110-03).

METHOD DETAILS

Cell Culture—$LNCaP^{shAR}$ cells stably transfected with a tetracycline-inducible anti-AR shRNA, as previously described (Cheng et al., 2006), were obtained as a gift from Dr. Paul S. Rennie. These cells were further modified via Lipofectamine 2000 (Invitrogen) transfection of a plasmid encoding a triple-probasin-driven herpes thymidine kinase (HSV-TK) and a Zeocin resistance cassette. A clonal population of this cell line derived from Zeocin (Invitrogen) selection and serial dilution in a 96-well plate, which we refer to as $LNCaP^{shAR/pATK}$, was subjected to total AR pathways suppression (TAPS): for two weeks the cells were grown in RPMI1640+5%CSS; at week 3, media was supplemented with 1 mg/mL doxycycline. Media was changed every 3–4 days and $LNCaP^{shAR/pATK}$ was maintained under TAPS for five months. A surviving colony of proliferating cells emerged. Following a 3-month expansion, this population of cells was treated with 50 μM ganciclovir (GCV; InvivoGen) for two weeks to eliminate any cells still robustly expressing an AR transcriptional program. We referred to the surviving population as $LNCaP^{APIPC}$.

Migration and Invasion Assays—Migration and invasion assays were performed as per protocol in Cultrex 96-well cell invasion/migration transwell plates (R&D Systems). RPMI1640+/−10%FBS was added to the lower chamber and 100,000 cells suspended in serum-free RPMI1640 were added to the top chamber. For invasion assays, membranes were coated with 0.2x BME. Fluorescence was measured on a BioTek Synergy2 multiwell plate reader and normalized to $LNCaP^{shAR/pATK}$ RPMI1640 serum-free control.

Cell Growth Assays—Cell growth was assayed by plating 5000 cells per well in a TC-treated 96-well black-sided, clear bottom plate (Corning). Media was changed every 48 hours and plates were collected at the reported timepoints and stored at −80°C. Plates for each experiment were assayed in batches using Cyquant (Invitrogen) to estimate cell viability as per manufacturer's protocol. Cells were treated with FGF8b (25 ng/mL; eBioscience) or PD173074 (1 μM; Tocris) or U0126 (25 μM). Additionally, cells were treated with doxycycline (1 mg/mL) and enzalutamide (5 μM) which was received as a gift from Medivation Inc.

Cells were plated as above and allowed to adhere for 24 hours then treated with various concentrations (as indicated in the figures) of CH-5183284 for 72 hours and assayed for apoptosis and viability using ApoLive Glo (Promega) following the manufactures instructions.

Conditioned Media—Serum-free phenol red-free Optimem (Invitrogen) was added to 80% confluent $LNCaP^{APIPC}$ and $LNCaP^{shAR/pATK}$ cultured in a tissue culture-treated T75 flask (Corning). Twenty-four hours later, media was collected and centrifuged for 5 minutes

at 5000 RPM to pellet cellular debris. The supernatant was added to an Amnicon Ultracel 3K centrifugal filter (Millipore) and concentrated as per manufacturer's instructions.

siRNA Transfection—Cells were plated at 5000 cells/well in a 96-well plate in 100 μl of phenol red-free Optimem supplemented with either 3% FBS or 3% CSS +1% PenStrep. Twenty-four hours after cell plating, cells were transfected with siRNA (Sigma) using RNAiMax lipofectamine reagent (Life Technologies) in 20 μl total volume. Cell viability was estimated 96 hours after transfection by adding Cell Titer-Glo (Promega) and measuring luminescence (RLUs) as per protocol on a BioTek Synergy2 multiwell plate reader. Luminescence measurements from wells transfected with an equimolar pool of 3xKif11 siRNAs was used to estimate transfection efficiency. Trans-fections performed in 6-well plates for RNA collection used scaled-up conditions from 96-well experiments, and cells were harvested 24 hours after transfection as described below. siRNA sequences can be found in the Key Resource Table.

RNA Collection and Quantitative Real-Time PCR—Cell culture total RNA was isolated from 6-well plates using an RNEasy kit (Qiagen) as per protocol. qRT-PCR reactions were performed in triplicate using an Applied Biosystems 7900 sequence detector with SYBR Green PCR master mix (Invitrogen). Primers were designed using PrimerQuest (IDT, and all reactions were normalized to the expression of the housekeeping gene RPL13A. A water negative control did not produce significant amplification product. PCR primer sequences can be found in the Table S1. Statistical analysis was performed using an unpaired two-sided Student's T-test to determine significance.

Protein Collection and Immunoblotting—Protein was collected from tissue culture by lysing adherent cells with a cell lysis buffer (1.5 M Urea, 1% SDS, 1% NP-40, 2% Tween20, 250 nM NaCl, PBS) supplemented with 1x phosphatase inhibitors (PhosStop, Roche Diagnostics) and a 1x protease inhibitor cocktail (Complete Mini, Roche Diagnostics). Protein was quantified per protocol using a bicinchoninic acid assay (Thermo Scientific). Normalized cell lysates were loaded onto a 12% NuPAGE Bis-Tris gel (Invitrogen) in MES buffer. Protein was transferred to nitrocellulose membranes using a semi-dry transfer apparatus and Tris/CAPS buffer. Immunoblots were probed with primary antibodies targeting AKT (Cell Signaling), phospho-AKT (Ser473; Cell Signaling), AR (Santa Cruz), Erk1/2 (Sigma), diphosphorylated-Erk1/2 (Sigma), FGF8b (R&D Systems), ID1 (Biocheck, Inc.), MEK1/2 (Sigma), phospho-MEK1 (Ser298; Upstate), or PSA (Dako). Horseradish-peroxidase conjugated secondary antibodies (Thermo Scientific) were used in conjugation with Supersignal West Pico Chemiluminescent substrate (Thermo Scientific) to visualize protein targets. Membranes were then stripped for 15 minutes in Stripping Buffer (Thermo Scientific) and re-probed with anti-Actin antibody (Santa Cruz Biotechnology) as a loading control.

Immunohistochemistry—PC metastases and xenograft tissues were fixed in buffered formalin (bone metastases were decalcified in 10% formic acid) and embedded in paraffin. Tissue microarrays (TMAs) were constructed using duplicate 1 mm diameter cores from these tissues. Five-micron thick sections of the TMAs were deparaffinized and rehydrated in

sequential xylene and graded ethanol. Antigen retrieval was performed in 10 mM citrate buffer (pH 6.0) in a pressure cooker. Endogenous peroxidase and avidin/biotin were blocked respectively (Vector Laboratories Inc.). Sections were then incubated with 5% normal goat-horse-chicken serum, incubated with the following primary antibody dilutions: anti-Androgen Receptor (Biogenex) 1:60, anti-Prostate-specific Antigen (Dako) 1:1000, anti-Chromogranin A (Dako) 1:100, anti-Synaptophysin (Santa Cruz) 1:200 and anti-human cytokeratin (Dako) 1:100. They were subsequently incubated with biotinylated secondary antibody (Vector Laboratories Inc.), followed by ABC reagent (Vector Laboratories Inc.), and stable DAB (Invitrogen Corp.). All sections were lightly counterstained with hematoxylin and mounted with Cytoseal XYL (Richard Allan Scientific). Mouse or rabbit IgG were used as negative controls.

AR CRISPR-Cas9 Editing—To create the sgRNA targeting exon 1 of AR, an sgRNA protospacer of CTCCGGACCTTACGGGGACATG was cloned in to the ESP3I enzyme (Thermo Fisher) sites of the lentivirus expression vector lentiCRISPRv2 (Addgene Plasmid #52961) using annealed oligos and AR_Exon1_sgRNA+: caccgCTCCGGACCTTACGGGGACATG and AR_Exon1_sgRNA-: aaacCATGTCCCCGTAAGGTCCGGAGc. To confirm on-target cutting, cells were transfected with lentiCRISPRv2:AR-sgRNA or GFP control using lipofectamine 2000 (Thermo Fisher) according to manufacturer's recommendation. After five days of selection with 1.5 μg/mL puromycin, genomic DNA was isolated using the DNeasy Blood & Tissue Kit (Qiagen) and amplified using Phusion High-Fidelity DNA Polymerase (New England Biolabs) and primers: AR-fwd CGACTTCACCGCACCTGATG and AR-rev AGGGCACGCAGCAGAAATTAG. On target CRISPR cutting was confirmed using T7 endonuclease I (New England Biolabs) heteroduplex cleavage assay to measure insertion/deletions, introduced via NHEJ-mediated double strand break repair of CRISPR activity.

PacMetUT1 cells were seeded in 10 cm dishes and transfected with lentiCRISPRv2:AR-sgRNA using lipofectamine 2000 (Thermo Fisher) according to manufacturer's protocols and recommendations. Cells were supplemented with 25 ng/mL FGF8b (R&D Systems) or PBS + 0.1% human BSA solvent control during five days of selection with 1.5 μg/mL puromycin. The surviving cells were replaced with fresh medium (RPMI 1640 10% FBS with or without FGF8b) and allowed to grow into colonies. Medium was changed once a week and FGF8b was replenished every three days. Approximately 5 weeks later, colonies were isolated from both FGF8b and PBS/BSA supplemented cells and allowed to expand for further analyses. Two colonies from cells treated with FGF8b were confirmed to be AR-negative by Western blot (GeneTex). These two colonies were referred to as the AR-null #1 and AR-null #2 sublines.

Transcript Profiling Methods—Cell line RNA was extracted using the Qiagen RNeasy Kit, (Qiagen Inc.), according to the manufacturer's protocol. On-column DNase digestion was performed. CRPC metastases RNA samples were prepared by reviewing a H&E of the frozen tissue block, followed by scoring the block with a razor so as to have as pure as possible sections of tumor. Cores were obtained from each of the bone metastases frozen tissue blocks that had been previously identified based upon review of H&E sections from

corresponding paraffin embedded blocks; adjacent areas of tumor were cored out of the frozen tissue blocks using a 2 mm diameter tissue punch in a −20 °C cryostat. Cores were homogenized in gentleMACS M Tubes (Miltenyi Biotec). Tissues were then isolated with RNA STAT-60 (Tel-Test). RNA concentration, purity, and integrity was assessed by NanoDrop (Thermo Fisher) and Agilent Bioanalyzer. Cell line RNA-seq libraries were constructed from 1 μg total RNA using the Illumina TruSeq RNA Library Prep Kit v2 according to the manufacturer's protocol. CRPC Metastases RNA-seq libraries were constructed from 1 μg total RNA using the Illumina TruSeq Stranded mRNA Library Prep Kit according to the manufacturer's protocol. Barcoded libraries were pooled and sequenced on the Illumina HiSeq 2500 generating 50 bp paired end reads. Sequencing reads were mapped to the hg19 human genome using TopHat v2.1.0. Gene level abundance was quantitated from the filtered human alignments in R using the Genomic Alignments v1.0.1 Bioconductor package.

QUANTIFICATION AND STATISTICAL ANALYSIS

Student's T-test was used to comparable significance between grouped quantitative data sets using GraphPad Prism 7.0 software. Differences were considered significant if $p \leq 0.05$. Differences in tumor volume (TV) between control and treated animals were calculated using unpaired t-tests with unequal variances, with significance set at $p \leq 0.05$.

Differential expression was assessed using transcript abundances as inputs to the edgeR v3.16.5 Bioconductor package in R. FDR and fold-change thresholds for significance are listed in the figure legends.

Unsupervised clustering of cell line expression profiles was performed in R on the 1000 most variable genes (calculated as the inter-quartile range of the $\log_2$ transcripts per million reads) using Euclidean distance and average-linkage. Clusters were visualized using the ape v4.1 Cran package.

The gene expression signature activity scores were calculated in R using the GSVA v1.24.0 Bioconductor package, using $\log_2$ transcripts per million reads as input. Pearson's correlation coefficient was used to study the relationships between variables shown in scatterplots using the cor.test function in R. The scatterplot3d v0.3–40 Cran package was used to plot three dimensional scatterplots.

Gene expression group comparisons were ranked by edgeR statistics and used to conduct Gene Set Enrichment Analysis using the GSEAv2.2.4 software to determine patterns of pathway activation in different phenotypic groups. We used the curated pathways and gene sets within MSigDBv6.0.

Genome-wide comparisons of copy number between DNPC and ARPC groups was performed using two-tailed fisher's exact tests using the fisher.test function in R. Proportions of tumors with somatic copy number alterations were compared, including high (greater than 1 copy) gain or homozygous loss.

DATA AND SOFTWARE AVAILABILITY

The RNA sequencing data has been deposited at the Gene Expression Omnibus (GEO) site: https://www.ncbi.nlm.nih.gov/geo/ under accession number GSE99381.

Supplementary Material

Refer to Web version on PubMed Central for supplementary material.

Acknowledgments

We are grateful to the patients and their families who participated in this study. We thank members of the P.S.N. laboratory for helpful advice and criticism. We thank Steve Plymate for helpful advice and assistance with analyses. We thank the FHCRC Genomics shared resource for assistance with RNA-seq experiments. We would also like to thank Yoshito Nakanishi for his advice, Bryce Lakely and Belinda Nguyen for technical assistance, Celestia Higano, Bruce Montgomery, Evan Yu, Heather Cheng, Funda-Vakar Lopez, Martine Roudier, Kristine Von Maltzan, Maria Tretiakova, and the rapid autopsy teams in the Urology Department at the University of Washington for their contributions to the Prostate Cancer Donor Rapid Autopsy Program. This work was supported by NIH awards: Prostate SPORE grant P50CA097186, P01 CA163227, DOD awards PC140794 and PC160662, a DF/HCC Mazzone award, the Institute for Prostate Cancer Research, the Richard M. Lucas Foundation, and a Challenge award from Movember and the Prostate Cancer Foundation.

References

Acevedo VD, Gangula RD, Freeman KW, Li R, Zhang Y, Wang F, Ayala GE, Peterson LE, Ittmann M, Spencer DM. Inducible FGFR-1 activation leads to irreversible prostate adenocarcinoma and an epithelial-to-mesenchymal transition. Cancer Cell. 2007; 12:559–571. [PubMed: 18068632]

Aihara M, Lebovitz RM, Wheeler TM, Kinner BM, Ohori M, Scardino PT. Prostate specific antigen and Gleason grade: an immunohistochemical study of prostate cancer. J. Urol. 1994; 151:1558–1564. [PubMed: 7514688]

Aparicio A, Tzelepi V, Araujo JC, Guo CC, Liang S, Troncoso P, Logothetis CJ, Navone NM, Maity SN. Neuroendocrine prostate cancer xenografts with large-cell and small-cell features derived from a single patient's tumor: morphological, immunohistochemical, and gene expression profiles. Prostate. 2011; 71:846–856. [PubMed: 21456067]

Arora VK, Schenkein E, Murali R, Subudhi SK, Wongvipat J, Balbas MD, Shah N, Cai L, Efstathiou E, Logothetis C, et al. Glucocorticoid receptor confers resistance to antiandrogens by bypassing androgen receptor blockade. Cell. 2013; 155:1309–1322. [PubMed: 24315100]

Aytes A, Mitrofanova A, Kinkade CW, Lefebvre C, Lei M, Phelan V, LeKaye HC, Koutcher JA, Cardiff RD, Califano A, et al. ETV4 promotes metastasis in response to activation of PI3-kinase and Ras signaling in a mouse model of advanced prostate cancer. Proc. Natl. Acad. Sci. USA. 2013; 110:E3506–E3515. [PubMed: 23918374]

Beltran H, Prandi D, Mosquera JM, Benelli M, Puca L, Cyrta J, Marotz C, Giannopoulou E, Chakravarthi BV, Varambally S, et al. Divergent clonal evolution of castration-resistant neuroendocrine prostate cancer. Nat. Med. 2016; 22:298–305. [PubMed: 26855148]

Beltran H, Rickman DS, Park K, Chae SS, Sboner A, MacDonald TY, Wang Y, Sheikh KL, Terry S, Tagawa ST, et al. Molecular characterization of neuroendocrine prostate cancer and identification of new drug targets. Cancer Discov. 2011; 1:487–495. [PubMed: 22389870]

Beltran H, Tomlins S, Aparicio A, Arora V, Rickman D, Ayala G, Huang J, True L, Gleave ME, Soule H, et al. Aggressive variants of castration-resistant prostate cancer. Clin. Cancer Res. 2014; 20:2846–2850. [PubMed: 24727321]

Carver BS, Chapinski C, Wongvipat J, Hieronymus H, Chen Y, Chandarlapaty S, Arora VK, Le C, Koutcher J, Scher H, et al. Reciprocal feedback regulation of PI3K and androgen receptor signaling in PTEN-deficient prostate cancer. Cancer Cell. 2011; 19:575–586. [PubMed: 21575859]

Cheng H, Snoek R, Ghaidi F, Cox ME, Rennie PS. Short hairpin RNA knockdown of the androgen receptor attenuates ligand-independent activation and delays tumor progression. Cancer Res. 2006; 66:10613–10620. [PubMed: 17079486]

Coppe JP, Itahana Y, Moore DH, Bennington JL, Desprez PY. Id-1 and Id-2 proteins as molecular markers for human prostate cancer progression. Clin. Cancer Res. 2004; 10:2044–2051. [PubMed: 15041724]

de Bono JS, Logothetis CJ, Molina A, Fizazi K, North S, Chu L, Chi KN, Jones RJ, Goodman OB Jr, Saad F, et al. Abiraterone and increased survival in metastatic prostate cancer. N. Engl. J. Med. 2011; 364:1995–2005. [PubMed: 21612468]

Delpuech O, Rooney C, Mooney L, Baker D, Shaw R, Dymond M, Wang D, Zhang P, Cross S, Veldman-Jones M, et al. Identification of pharmacodynamic transcript biomarkers in response to FGFR inhibition by AZD4547. Mol. Cancer Ther. 2016; 15:2802–2813. [PubMed: 27550940]

Doctor SM, Tsao CK, Godbold JH, Galsky MD, Oh WK. Is prostate cancer changing?: evolving patterns of metastatic castration-resistant prostate cancer. Cancer. 2014; 120:833–839. [PubMed: 25302607]

Erbersdobler A, Isbarn H, Steiner I, Schlomm T, Chun F, Mirlacher M, Sauter G. Predictive value of prostate-specific antigen expression in prostate cancer: a tissue microarray study. Urology. 2009; 74:1169–1173. [PubMed: 19476978]

Feldman BJ, Feldman D. The development of androgen-independent prostate cancer. Nat. Rev. Cancer. 2001; 1:34–45. [PubMed: 11900250]

Feng S, Wang J, Zhang Y, Creighton CJ, Ittmann M. FGF23 promotes prostate cancer progression. Oncotarget. 2015; 6:17291–17301. [PubMed: 26019137]

Gioeli D, Mandell JW, Petroni GR, Frierson HF Jr, Weber MJ. Activation of mitogen-activated protein kinase associated with prostate cancer progression. Cancer Res. 1999; 59:279–284. [PubMed: 9927031]

Gregory CW, Whang YE, McCall W, Fei X, Liu Y, Ponguta LA, French FS, Wilson EM, Earp HS 3rd. Heregulin-induced activation of HER2 and HER3 increases androgen receptor transactivation and CWR-R1 human recurrent prostate cancer cell growth. Clin. Cancer Res. 2005; 11:1704–1712. [PubMed: 15755991]

Hänzelmann S, Castelo R, Guinney J. GSVA: gene set variation analysis for microarray and RNA-seq data. BMC Bioinformatics. 2013; 14:7. [PubMed: 23323831]

Hieronymus H, Lamb J, Ross KN, Peng XP, Clement C, Rodina A, Nieto M, Du J, Stegmaier K, Raj SM, et al. Gene expression signature-based chemical genomic prediction identifies a novel class of HSP90 pathway modulators. Cancer Cell. 2006; 10:321–330. [PubMed: 17010675]

Kim D, Pertea G, Trapnell C, Pimentel H, Kelley R, Salzberg SL. TopHat2: accurate alignment of transcriptomes in the presence of insertions, deletions and gene fusions. Genome Biol. 2013; 14:R36. [PubMed: 23618408]

Ku SY, Rosario S, Wang Y, Mu P, Seshadri M, Goodrich ZW, Goodrich MM, Labbe DP, Gomez EC, Wang J, et al. Rb1 and Trp53 cooperate to suppress prostate cancer lineage plasticity, metastasis, and antiandrogen resistance. Science. 2017; 355:78–83. [PubMed: 28059767]

Kumar A, Coleman I, Morrissey C, Zhang X, True LD, Gulati R, Etzioni R, Bolouri H, Montgomery B, White T, et al. Substantial interindividual and limited intraindividual genomic diversity among tumors from men with metastatic prostate cancer. Nat. Med. 2016; 22:369–378. [PubMed: 26928463]

Langenfeld EM, Langenfeld J. Bone morphogenetic protein-2 stimulates angiogenesis in developing tumors. Mol. Cancer Res. 2004; 2:141–149. [PubMed: 15037653]

Lawrence M, Huber W, Pagès H, Aboyoun P, Carlson M, Gentleman R, Morgan MT, Carey VJ. Software for computing and annotating genomic ranges. PLoS Comput. Biol. 2013; 9:e1003118. [PubMed: 23950696]

Lawson DA, Zong Y, Memarzadeh S, Xin L, Huang J, Witte ON. Basal epithelial stem cells are efficient targets for prostate cancer initiation. Proc. Natl. Acad. Sci. USA. 2010; 107:2610–2615. [PubMed: 20133806]

Li ZG, Mathew P, Yang J, Starbuck MW, Zurita AJ, Liu J, Sikes C, Multani AS, Efstathiou E, Lopez A, et al. Androgen receptor-negative human prostate cancer cells induce osteogenesis in mice through FGF9-mediated mechanisms. J. Clin. Invest. 2008; 118:2697–2710. [PubMed: 18618013]

Ligges U, Machler M. Scatterplot3d: an R package for visualizing multivariate data. J. Stat. Softw. 2003; 8:1–20.

Ling YX, Tao J, Fang SF, Hui Z, Fang QR. Downregulation of Id1 by small interfering RNA in prostate cancer PC3 cells in vivo and in vitro. Eur. J. Cancer Prev. 2011; 20:9–17. [PubMed: 20881502]

MacArthur CA, Lawshe A, Shankar DB, Heikinheimo M, Shackleford GM. FGF-8 isoforms differ in NIH3T3 cell transforming potential. Cell Growth Differ. 1995; 6:817–825. [PubMed: 7547503]

Mohammadi M, Froum S, Hamby JM, Schroeder MC, Panek RL, Lu GH, Eliseenkova AV, Green D, Schlessinger J, Hubbard SR. Crystal structure of an angiogenesis inhibitor bound to the FGF receptor tyrosine kinase domain. EMBO J. 1998; 17:5896–5904. [PubMed: 9774334]

Montgomery RB, Mostaghel EA, Vessella R, Hess DL, Kalhorn TF, Higano CS, True LD, Nelson PS. Maintenance of intratumoral androgens in metastatic prostate cancer: amechanism for castration-resistant tumor growth. Cancer Res. 2008; 68:4447–4454. [PubMed: 18519708]

Mu P, Zhang Z, Benelli M, Karthaus WR, Hoover E, Chen CC, Wongvipat J, Ku SY, Gao D, Cao Z, et al. SOX2 promotes lineage plasticity and antiandrogen resistance in TP53- and RB1-deficient prostate cancer. Science. 2017; 355:84–88. [PubMed: 28059768]

Mulholland DJ, Kobayashi N, Ruscetti M, Zhi A, Tran LM, Huang J, Gleave M, Wu H. Pten loss and RAS/MAPK activation cooperate to promote EMT and metastasis initiated from prostate cancer stem/progenitor cells. Cancer Res. 2012; 72:1878–1889. [PubMed: 22350410]

Mulholland DJ, Tran LM, Li Y, Cai H, Morim A, Wang S, Plaisier S, Garraway IP, Huang J, Graeber TG, Wu H. Cell autonomous role of PTEN in regulating castration-resistant prostate cancer growth. Cancer Cell. 2011; 19:792–804. [PubMed: 21620777]

Nakanishi Y, Akiyama N, Tsukaguchi T, Fujii T, Sakata K, Sase H, Isobe T, Morikami K, Shindoh H, Mio T, et al. The fibroblast growth factor receptor genetic status as a potential predictor of the sensitivity to CH5183284/Debio 1347, a novel selective FGFR inhibitor. Mol. Cancer Ther. 2014; 13:2547–2558. [PubMed: 25169980]

Nelson PS, Clegg N, Arnold H, Ferguson C, Bonham M, White J, Hood L, Lin B. The program of androgen-responsive genes in neoplastic prostate epithelium. Proc. Natl. Acad. Sci. USA. 2002; 99:11890–11895. [PubMed: 12185249]

Oka H, Chatani Y, Kohno M, Kawakita M, Ogawa O. Constitutive activation of the 41- and 43-kDa mitogen-activated protein (MAP) kinases in the progression of prostate cancer to an androgen-independent state. Int. J. Urol. 2005; 12:899–905. [PubMed: 16323984]

Ouyang XS, Wang X, Ling MT, Wong HL, Tsao SW, Wong YC. Id-1 stimulates serum independent prostate cancer cell proliferation through inactivation of p16(INK4a)/pRB pathway. Carcinogenesis. 2002; 23:721–725. [PubMed: 12016143]

Paradis E, Claude J, Strimmer K. APE: analyses of phylogenetics and evolution in R language. Bioinformatics. 2004; 20:289–290. [PubMed: 14734327]

Passiatore G, Gentilella A, Rom S, Pacifici M, Bergonzini V, Peruzzi F. Induction of Id-1 by FGF-2 involves activity of EGR-1 and sensitizes neuroblastoma cells to cell death. J. Cell Physiol. 2011; 226:1763–1770. [PubMed: 21506108]

Perk J, Iavarone A, Benezra R. Id family of helix-loop-helix proteins in cancer. Nat. Rev. Cancer. 2005; 5:603–614. [PubMed: 16034366]

Robinson MD, McCarthy DJ, Smyth GK. edgeR: a Bioconductor package for differential expression analysis of digital gene expression data. Bioinformatics. 2010; 26:139–140. [PubMed: 19910308]

Robinson D, Van Allen EM, Wu YM, Schultz N, Lonigro RJ, Mosquera JM, Montgomery B, Taplin ME, Pritchard CC, Attard G, et al. Integrative clinical genomics of advanced prostate cancer. Cell. 2015; 161:1215–1228. [PubMed: 26000489]

Rodriguez-Berriguete G, Fraile B, Martinez-Onsurbe P, Olmedilla G, Paniagua R, Royuela M. MAP kinases and prostate cancer. J. Signal. Transduct. 2012; 2012:169170. [PubMed: 22046506]

Roudier MP, True LD, Higano CS, Vesselle H, Ellis W, Lange P, Vessella RL. Phenotypic heterogeneity of end-stage prostate carcinoma metastatic to bone. Hum. Pathol. 2003; 34:646–653. [PubMed: 12874759]

Sanjana NE, Shalem O, Zhang F. Improved vectors and genome-wide libraries for CRISPR screening. Nat. Methods. 2014; 11:783–784. [PubMed: 25075903]

Scher HI, Fizazi K, Saad F, Taplin ME, Sternberg CN, Miller K, de Wit R, Mulders P, Chi KN, Shore ND, et al. Increased survival with enzalutamide in prostate cancer after chemotherapy. N. Engl. J. Med. 2012; 367:1187–1197. [PubMed: 22894553]

Shah RB, Mehra R, Chinnaiyan AM, Shen R, Ghosh D, Zhou M, Macvicar GR, Varambally S, Harwood J, Bismar TA, et al. Androgen-independent prostate cancer is a heterogeneous group of diseases: lessons from a rapid autopsy program. Cancer Res. 2004; 64:9209–9216. [PubMed: 15604294]

Sharma P, Patel D, Chaudhary J. Id1 and Id3 expression is associated with increasing grade of prostate cancer: Id3 preferentially regulates CDKN1B. Cancer Med. 2012; 1:187–197. [PubMed: 23342268]

Snoek R, Cheng H, Margiotti K, Wafa LA, Wong CA, Wong EC, Fazli L, Nelson CC, Gleave ME, Rennie PS. In vivo knockdown of the androgen receptor results in growth inhibition and regression of well-established, castration-resistant prostate tumors. Clin. Cancer Res. 2009; 15:39–47. [PubMed: 19118031]

Sobel RE, Sadar MD. Cell lines used in prostate cancer research: a compendium of old and new lines —part 2. J. Urol. 2005; 173:360–372. [PubMed: 15643173]

Subramanian A, Tamayo P, Mootha VK, Mukherjee S, Ebert BL, Gillette MA, Paulovich A, Pomeroy SL, Golub TR, Lander ES, et al. Gene set enrichment analysis: a knowledge-based approach for interpreting genome-wide expression profiles. Proc. Natl. Acad. Sci. USA. 2005; 102:15545–15550. [PubMed: 16199517]

Taylor BS, Schultz N, Hieronymus H, Gopalan A, Xiao Y, Carver BS, Arora VK, Kaushik P, Cerami E, Reva B, et al. Integrative genomic profiling of human prostate cancer. Cancer Cell. 2010; 18:11–22. [PubMed: 20579941]

Troyer DA, Tang Y, Bedolla R, Adhvaryu SG, Thompson IM, Abboud-Werner S, Sun LZ, Friedrichs WE, deGraffenried LA. Characterization of PacMetUT1, a recently isolated human prostate cancer cell line. Prostate. 2008; 68:883–892. [PubMed: 18361412]

Tzelepi V, Zhang J, Lu JF, Kleb B, Wu G, Wan X, Hoang A, Efstathiou E, Sircar K, Navone NM, et al. Modeling a lethal prostate cancer variant with small-cell carcinoma features. Clin. Cancer Res. 2012; 18:666–677. [PubMed: 22156612]

Ueda T, Mawji NR, Bruchovsky N, Sadar MD. Ligand-inde-pendent activation of the androgen receptor by interleukin-6 and the role of steroid receptor coactivator-1 in prostate cancer cells. J. Biol. Chem. 2002; 277:38087–38094. [PubMed: 12163482]

Wan X, Corn PG, Yang J, Palanisamy N, Starbuck MW, Efstathiou E, Tapia EM, Zurita AJ, Aparicio A, Ravoori MK, et al. Prostate cancer cell-stromal cell crosstalk via FGFR1 mediates antitumor activity of dovitinib in bone metastases. Sci. Transl. Med. 2014; 6:252ra122.

Wang W, Epstein JI. Small cell carcinoma of the prostate. A morphologic and immunohistochemical study of 95 cases. Am. J. Surg. Pathol. 2008; 32:65–71. [PubMed: 18162772]

Wu YM, Su F, Kalyana-Sundaram S, Khazanov N, Ateeq B, Cao X, Lonigro RJ, Vats P, Wang R, Lin SF, et al. Identification of target-able FGFR gene fusions in diverse cancers. Cancer Discov. 2013; 3:636–647. [PubMed: 23558953]

Yang L, Wang L, Lin HK, Kan PY, Xie S, Tsai MY, Wang PH, Chen YT, Chang C. Interleukin-6 differentially regulates androgen receptor transactivation via PI3K–Akt, STAT3, and MAPK, three distinct signal pathways in prostate cancer cells. Biochem. Biophys. Res. Commun. 2003; 305:462–469. [PubMed: 12763015]

Zegarra-Moro OL, Schmidt LJ, Huang H, Tindall DJ. Disruption of androgen receptor function inhibits proliferation of androgen-re-fractory prostate cancer cells. Cancer Res. 2002; 62:1008–1013. [PubMed: 11861374]

Zhang XQ, Kondrikov D, Yuan TC, Lin FF, Hansen J, Lin MF. Receptor protein tyrosine phosphatase alpha signaling is involved in androgen depletion-induced neuroendocrine differentiation of androgen-sensitive LNCaP human prostate cancer cells. Oncogene. 2003; 22:6704–6716. [PubMed: 14555984]

Zou M, Toivanen R, Mitrofanova A, Floc'h N, Hayati S, Sun Y, Le Magnen C, Chester D, Mostaghel EA, Califano A, et al. Transdifferentiation as a mechanism of treatmentresistance in a mouse

model of castration-resistant prostate cancer. Cancer Discov. 2017; 7:736–749. [PubMed: 28411207]

Highlights

- The frequency of double-negative (AR-null; NE-null) prostate cancer is increasing
- FGF and MAPK pathways are active in AR-null prostate cancer
- Autocrine and paracrine FGF pathway activation can bypass AR dependence
- Targeting the FGF and MAPK pathways can repress AR-null prostate cancer

Significance

Targeting AR signaling in metastatic PC commonly produces robust clinical responses. However, disease progression is nearly universal. Potent AR antagonists appear to be shifting the phenotypes of resistant PCs to tumors that are devoid of AR activity, but the drivers of these resistant carcinomas are not known. Here we report that autocrine and paracrine FGF signaling is capable of bypassing a requirement for AR, and find that FGF and MAPK pathways are active in metastatic AR-null PCs. Suppressing FGF and MAPK inhibits the growth of AR-null PC indicating that targeting the FGF axis may represent a therapeutic approach for those cancers resistant to AR-directed therapies and may circumvent treatment resistance if combined with initial AR pathway blockade.

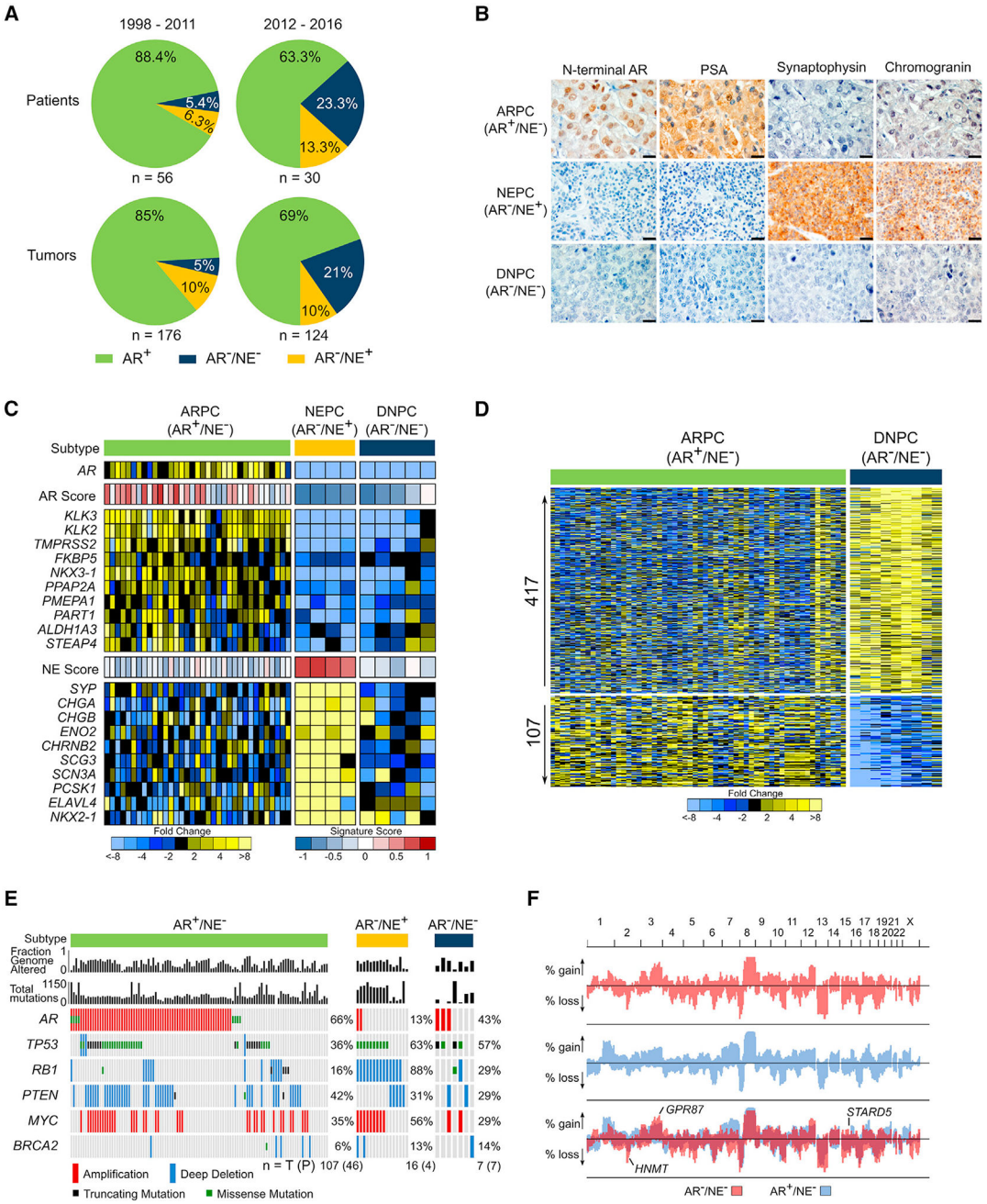

Figure 1. Molecular Features of AR-Null Neuroendocrine-Null Prostate Cancer

(A) The frequency of AR-active prostate cancers (ARPC), neuroendocrine prostate cancers (NEPC), and double-negative AR-null/neuroendocrine-null prostate cancers (DNPC) in men with metastatic CRPC evaluated in consecutive tissue acquisition necropsies from 1998 to 2016. Numbers of tumors and patients in each cohort is shown.

(B) Representative immunohistochemical stains for AR, PSA, synaptophysin and chromogranin used to classify metastases as ARPC, NEPC, or DNPC. Scale bars, 20 μm.

(C) RNA sequencing-based measurements of transcripts comprising AR-regulated genes and neuroendocrine phenotype-associated genes in metastatic tumors from men with CRPC.

Signature scores are shown above each gene set. Expression profile of one representative tumor per patient is shown, (AR^+/NE^-, n = 35; AR^-/NE^+, n = 4; AR^-/NE^-, n = 5.)
(D) Differentially expressed genes in ARPC compared with DNPC (5-fold difference; q value <0.0001). Transcript abundance was determined by RNA sequencing and analyzed for differential expression using the Bioconductor edgeR software (ARPC, n = 58 tumors from 35 men; DNPC, n = 9 tumors from 5 men).
(E) The frequency of recurrent genomic aberrations in the CRPC subtypes of AR^+/NE^- (ARPC), AR^-/NE^+ (NEPC), and AR^-/NE^- (DNPC) determined by aCGH and exome sequencing. Status of individual tumors and percentage altered in each group is shown, with numbers of patients (P) and tumors (T) below the plot.
(F) Frequency of copy-number alterations (CNAs) determined by genome-wide array CGH. Copy-number gains and losses in ARPC (blue), DNPC (red), and shared (purple). Three genes (*HNMT, GPR87*, and *STARD5*) were significant by two-tailed Fisher's exact tests comparing the proportion of high copy gains or homozygous losses between the groups ($p < 0.05$) and also exhibited concordant differential mRNA expression by two-sample t test ($p < 0.05$). (DNPC, n = 8 tumors from 8 individuals; ARPC, n = 118 tumors from 52 individuals).
See also Figure S1.

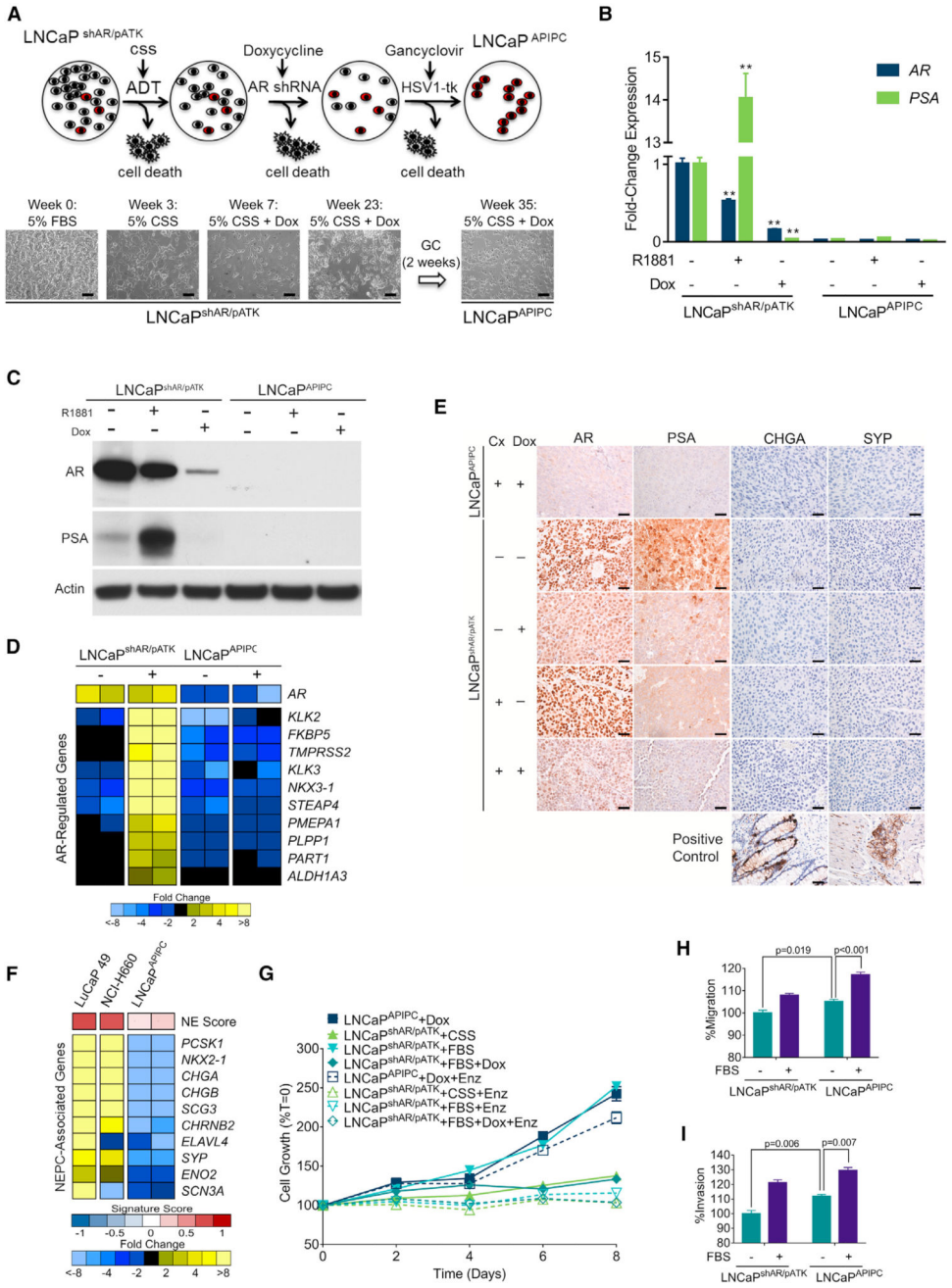

Figure 2. Characterization of a Model of AR Program-Independent Prostate Cancer

(A) LNCaP cells with a doxycycline (Dox)-inducible shRNA targeting the AR (shAR) and an androgen-driven thymidine kinase gene (pATK) were starved of androgens (ADT) and treated with Dox to induce the AR-directed shRNA, then treated with ganciclovir to eliminate cells with AR-driven thymidine kinase expression. Scale bars, 10 μm.

(B) qRT-PCR analysis of AR and PSA expression in LNCaP$^{shAR/pATK}$ and LNCaP^{APIPC} with 1 nM R1881 or 1 μg/mL Dox treatment. Significance was determined by Student's t test and data are presented as mean ± SEM (n = 4 replicates per data point); **p < 0.01.

(C) AR and PSA immunoblots of cell lysates from LNCaP$^{shAR/pATK}$ and LNCaP^{APIPC} cultured in androgen-deprived conditions and treated with or without R1881 and with or without Dox.

(D) Quantitation of AR-regulated transcripts following treatment with the synthetic androgen R1881 (+) in parental LNCaP$^{shAR/pATK}$ and LNCaP^{APIPC} cells. Measurements were made by RNA sequencing (n = 2 biological replicates per group).

(E) Immunohistochemical analysis of AR, PSA, CHGA, and SYP in parental LNCaP$^{shAR/pATK}$ and LNCaP^{APIPC} xenografts. Cx, castration; Dox, doxycycline. Scale bars, 10 μm.

(F) Expression of neuroendocrine-associated transcripts in the NEPC LuCaP49 PDX model, NEPC NCI-H660 cell line, and LNCaP^{APIPC} cells. Measurements were made by RNA sequencing (RNA-seq) (n = 2 biological replicates of LNCaP^{APIPC} cells, 1 each of LuCaP49 and NCI-H660).

(G) LNCaP^{APIPC} grown in androgen- and AR-depleted conditions were treated with vehicle (DMSO) or 5 μM enzalutamide (ENZ). Growth was compared with parental LNCaP$^{shAR/pATK}$ cells in charcoal stripped serum (CSS), fetal bovine serum (FBS), or FBS + 1 μg/mL Dox ± ENZ. Solid lines, with DMSO vehicle; dotted lines, with ENZ. All values are normalized to day 0. Data are presented as mean ± SEM (n = 5 per data point).

(H and I) Transwell migration (H) and invasion assays (I) of LNCaP$^{shAR/pATK}$ and LNCaP^{APIPC} at baseline (no FBS gradient) and in response to a serum (FBS) gradient. Significance was determined using Student's t test and data are presented as mean ± SEM (n = 4).

See also Figure S2.

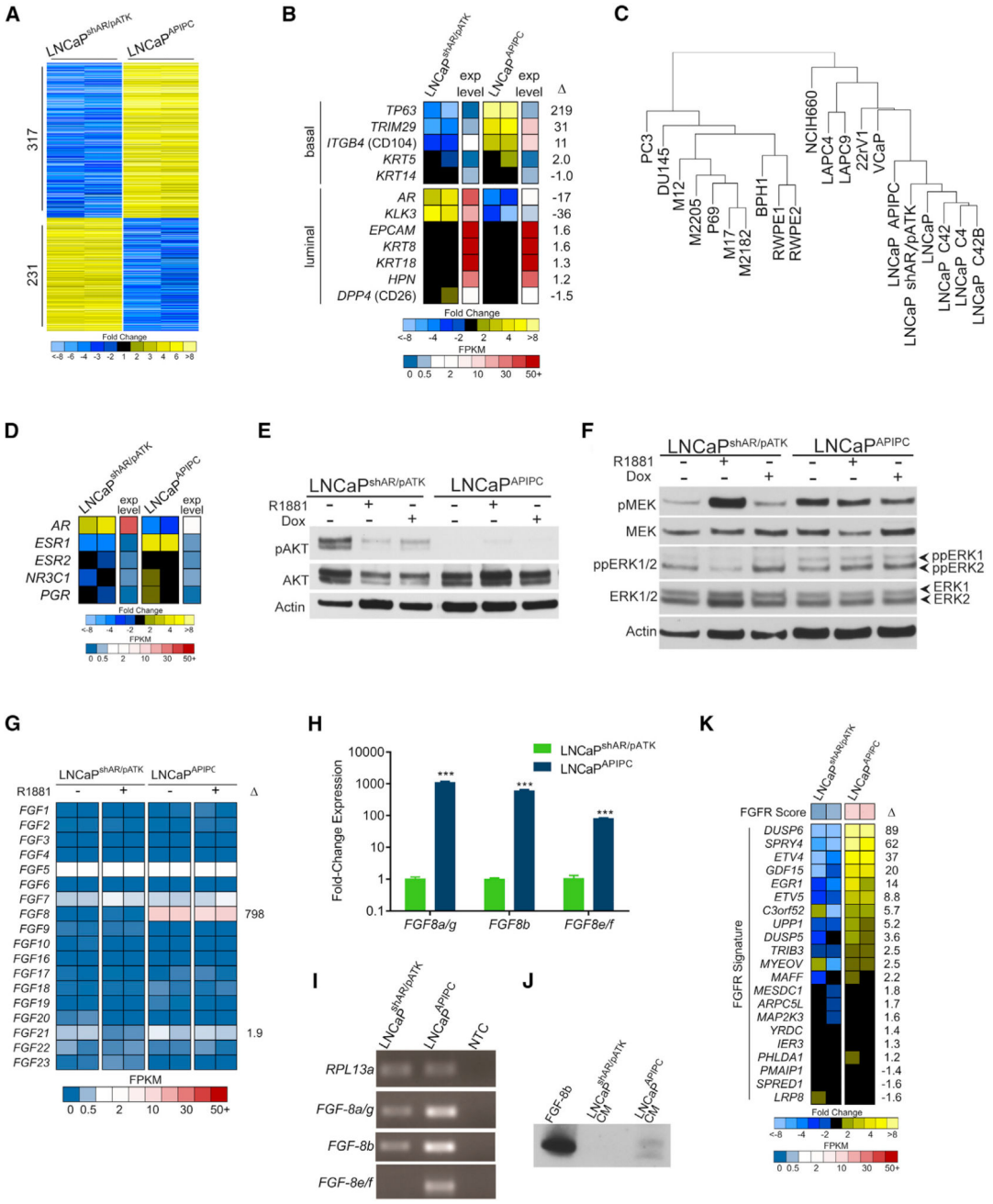

Figure 3. Assessments of AKT, MAPK, and FGF Pathway Activity in the LNCaP^{APIPC} Model of DNPC

(A) Genome-wide assessment of transcripts differentially expressed between LNCaP$^{shAR/pATK}$ and LNCaP^{APIPC} cells as measured by RNA-seq. Shown are 548 genes with q values of <0.001 and fold changes of ≥10 (n = 2 biological replicates per group).

(B) Measurements of luminal and basal cell gene expression in LNCaP^{APIPC} cells. Relative ratios of RNA-seq transcript abundances are shown, along with mean FPKM (fragments per kilobase of transcript per million mapped reads) values (n = 2 biological replicates per group).

(C) Unsupervised cluster analysis of gene expression profiles across prostate cancer cell lines associates LNCaP^{APIPC} cells with LNCaP cells and sublines. One replicate of each cell line used to cluster RNA-seq profiles of the top 1,000 most variable genes.
(D) Expression of nuclear hormone receptors determined by RNA-seq of LNCaP$^{shAR/pATK}$ and LNCaP^{APIPC} cells. Relative ratios of RNA-seq transcript abundances are shown, along with mean FPKM values. Two independent biological replicates were sequenced.
(E) PI3K pathway signaling was assessed by probing LNCaP^{APIPC} and LNCaP$^{shAR/pATK}$ cell lysates with antibodies to AKT and phosphorylated AKT.
(F) MAPK pathway signaling was assessed by probing LNCaP^{APIPC} and LNCaP$^{shAR/pATK}$ cell lysates with antibodies to MEK, phosphorylated MEK, ERK1/2, and dually phosphorylated ERK1/2.
(G) Levels of transcripts encoding FGFs were assessed in LNCaP$^{shAR/pATK}$ and LNCaP^{APIPC} cells by RNA-seq with or without R1881 androgen treatment. Two replicates of each line and treatment were measured, and fold difference between LNCaP$^{shAR/pATK}$ and LNCaP^{APIPC} cells is shown for FGF8 and FGF21.
(H) Transcript levels of FGF8 mRNAs were measured by qRT-PCR in LNCaP$^{shAR/pATK}$ and LNCaP^{APIPC}. Significance was determined by Student's t test and data are presented as mean ± SEM (n = 3 replicates per data point). ***$p < 0.00001$.
(I) qRT-PCR reaction products, visualized by agarose gel electrophoresis, confirms single-band amplification by each isoform-specific primer pair.
(J) Assessment of FGF8b protein in conditioned medium (CM) from LNCaP$^{shAR/pATK}$ and LNCaP^{APIPC} by immunoblotting with an FGF8b–specific antibody.
(K) Expression of genes associated with FGFR pathway activity measured by RNA-seq of LNCaP$^{shAR/pATK}$ and LNCaP^{APIPC} cells. Two independent biological replicates were sequenced.
See also Figures S3 and S4.

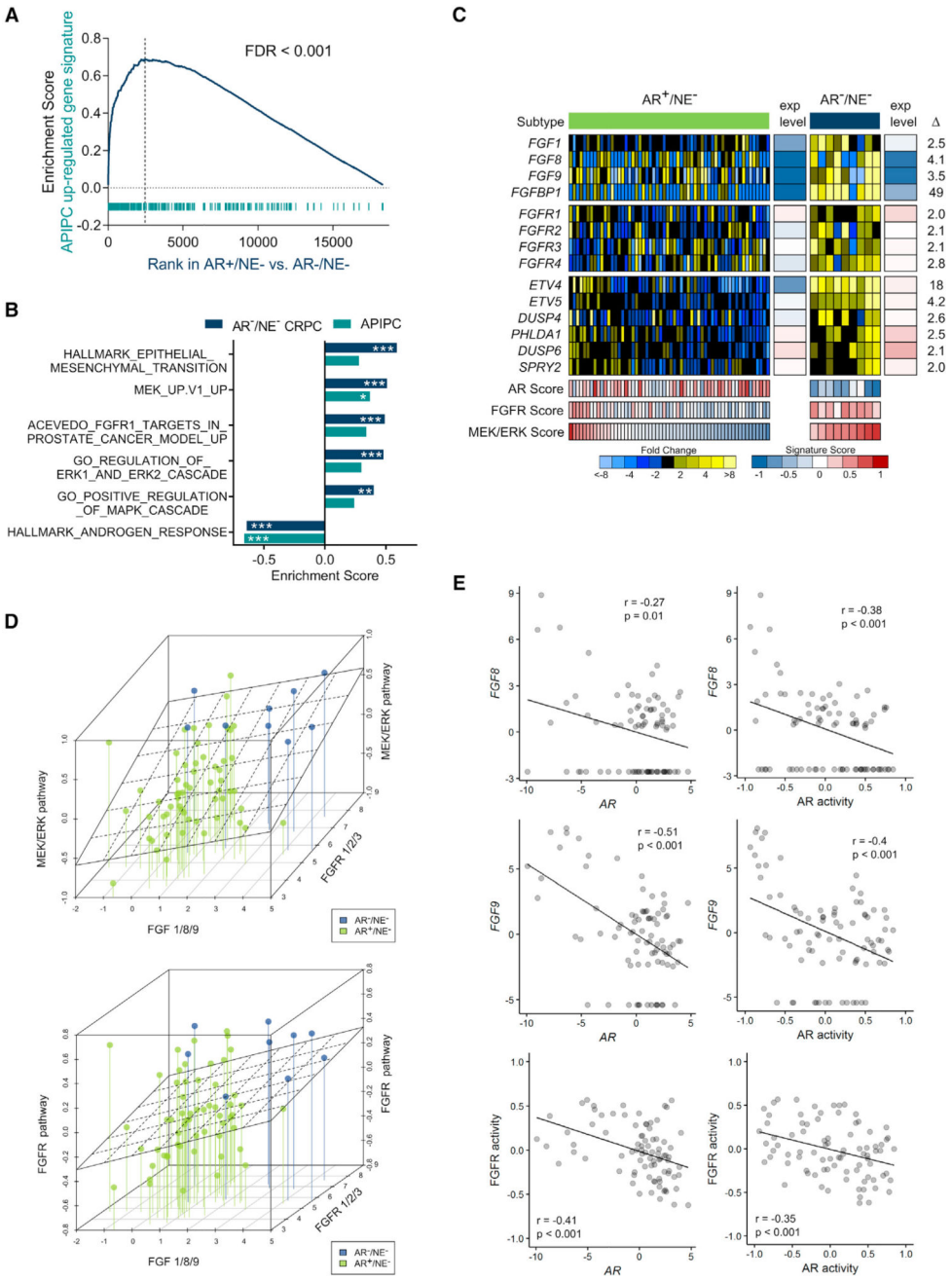

Figure 4. Assessments of FGF and MAPK Activity in Metastatic CRPC

(A) Analyses of transcripts differentially expressed between LNCaP$^{shAR/pATK}$ and LNCaP^{APIPC} in DNPC and ARPC metastases (FDR < 0.001, pre-ranked GSEA).

(B) GSEA demonstrates significant positive associations with FGF, MAPK, MEK/ERK, and EMT pathways and negative enrichment for AR response in DNPC metastases (***FDR < 0.0005, **FDR < 0.005, *FDR < 0.05, pre-ranked GSEA).

(C) Expression of FGF ligands, FGF receptors, and genes comprising an MEK/ERK activity signature. Relative ratios of RNA-seq transcript abundances are shown, along with mean

FPKM values and signature scores (AR^+/NE^-, n = 58 tumors from 35 men; AR^-/NE^-, n = 9 tumors from 5 men).

(D) Plot of CRPC metastasis triangulated by the highest transcript level of FGF1, 8, or 9 (x axis), MEK/ERK pathway activity score or FGFR pathway activity score (y axis), and highest transcript level of FGFR1, 2, or 3 (z axis). Lines anchor MEK/ERK activity to lowest level to assist in visualizing activity on the y axis. A linear regression analysis of pathway score versus ligands and receptors is plotted as a plane (AR^+/NE^-, n = 58 tumors from 35 men; AR^-/NE^-, n = 9 tumors from 5 men).

(E) Correlation of *FGF8* and *FGF9* transcript levels and FGFR pathway activity and AR activity scores assessed in 85 CRPC metastases from 50 men by RNA-seq. Pearson's correlation coefficient and p value are indicated on each plot.

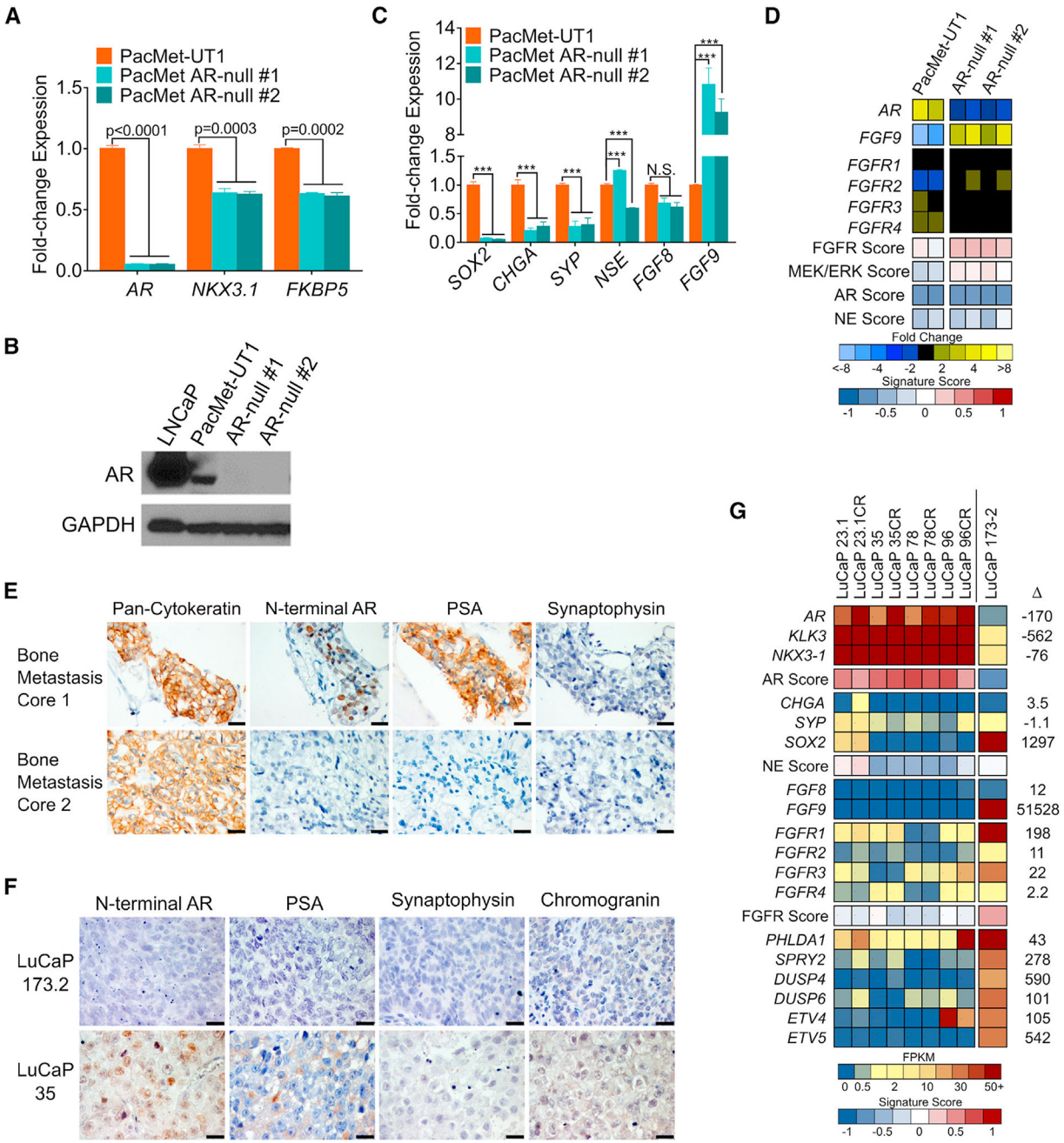

Figure 5. FGF Pathway and MAPK Activity in Cell Line and PDX Models of DNPC

(A) Quantitation of the indicated transcripts by qRT-PCR in parental PacMet-UT1 cells and two independent PacMet-UT1 clones propagated after CRISPR/Cas9-mediated AR deletion.

(B) Western immunoblot of AR protein in the indicated cell lines.

(C) Quantitation of the indicated transcripts by qRT-PCR in the indicated cell lines. ***p < 0.0001. N.S., not significant.

(D) Expression of genes reflecting the activity of AR, neuroendocrine (NE), FGFR, and MAPK signaling in parental PacMet-UT1 cells and AR-null sublines. Measurements were derived from RNA-seq (n = 2 biological replicates per group).

(E) Cytokeratin, AR, PSA, and synaptophysin IHC in two independent rib metastases obtained from a patient with mCRPC. Scale bars, 20 μm.
(F) AR, PSA, synaptophysin, and chromogranin IHC in the LuCaP173.2 PDX model derived from rib metastasis core 2 (E) with comparisons with the AR-positive LuCaP35 PDX line. Scale bars, 20 μm.
(G) Expression of genes comprising the AR program, neuroendocrine (NE) program, and FGFR program in AR-positive castration-sensitive and castration-resistant (CR) PDX models (LuCaP23.1, LuCaP35, LuCaP78, and LuCaP96) and the AR-null, NE-null LuCaP173.2 PDX line. Measurements were derived from RNA-seq (n = one tumor from each LuCaP line.).
For (A) and (C), significance was determined by Student's t test and data are presented as mean ± SEM (n = 3 replicates per data point). See also Figure S5.

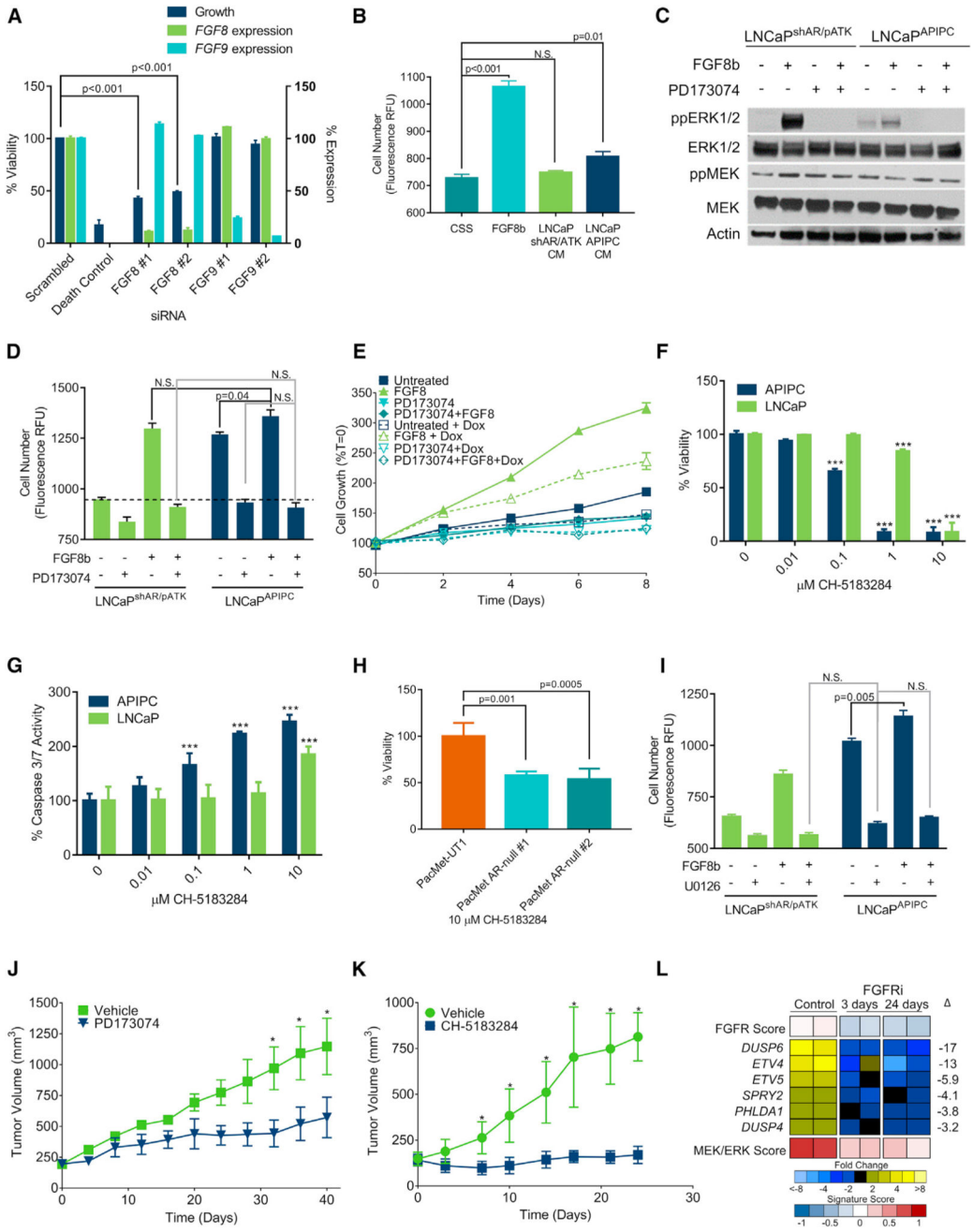

Figure 6. FGF Activates MAPK Signaling and Bypasses a Requirement for AR Activity in Promoting Prostate Cancer Growth

(A) Quantitation of cell viability and gene expression 96 hr after transfecting LNCaP^{APIPC} cells with siRNA pools specific for the indicated target.

(B) LNCaP$^{shAR/pATK}$ were cultured for 4 daysin androgen-depleted medium and treated with 25ng/mL FGF8b, CM from LNCaP$^{shAR/pATK}$, or LNCaP^{APIPC} cells. Cell number was determined using Cyquant.

(C) LNCaP$^{shAR/pATK}$ and LNCaP^{APIPC} were treated with 1 μM PD173074 or vehicle and 25 ng/mL FGF8 or vehicle and cell lysates were evaluated for MAPK signaling via immunoblotting for ppERK1/2.

(D) LNCaP$^{shAR/pATK}$ and LNCaP^{APIPC} were cultured in androgen-deprived conditions and treated with ±25 ng/mL FGF8b and ±1 μM PD173074. N.S., not significant. Dashed line indicates unstimulated LNCaP$^{shAR/pATK}$ (n = 3 replicates per data point).
(E) LNCaP$^{shAR/pATK}$ cells were cultured in androgen-depleted medium ±25 ng/mL FGF8, ±1 μM PD173074, and ±1 μg/mL Dox. Solid lines, no Dox; dotted lines, with Dox. Cell number was determined using Cyquant, and values were normalized to day 0.
(F and G) LNCaP and LNCaP^{APIPC} were treated with the indicated concentrations of CH-5183284, and cell viability (F) and apoptosis (G) were measured after 72 hr by ApoLive Glo (n = 3 replicates per data point). ***p < 0.001.
(H) PacMet-UT1 cells and AR-null derivatives were treated with 10 μM CH-5183284, and cell viability was determined by CellTiter Glo after 72 hr.
(I) LNCaP$^{shAR/pATK}$ and LNCaP^{APIPC} cultured in androgen-depleted conditions were treated with FGF8b or vehicle with or without 25 μM U0126 or vehicle. Cell number was determined using Cyquant.
(J) LNCaP^{APIPC} cells were inoculated subcutaneously in castrate SCID mice receiving Dox-supplemented feed. When tumors reached 200 mm^3 in size, treatment was initiated with the FGFR antagonist PD173074 or vehicle control. Tumor volumes were measured every 2 days (n = 5). *p < 0.01.
(K) LuCaP173.2 tumors were implanted subcutaneously in castrate SCID mice. When tumors reached 200 mm^3 in size, treatment was initiated with the FGFR antagonist CH-5183284 or vehicle control. Tumor volumes were measured every 2 days (n = 15). *p < 0.01.
(L) Quantitation of FGFR and MEK/ERK pathway gene expression in LuCaP173.2 tumors treated with vehicle or CH-5183284 sampled 3 days or 24 days after the initiation of treatment. Transcripts were quantitated by RNA-seq of two independent tumors.
Significance was determined by Student's t test and data are presented as mean ± SEM. For (A), (B), and (D) to (I), n = 3 replicates per data point. See also Figure S6.

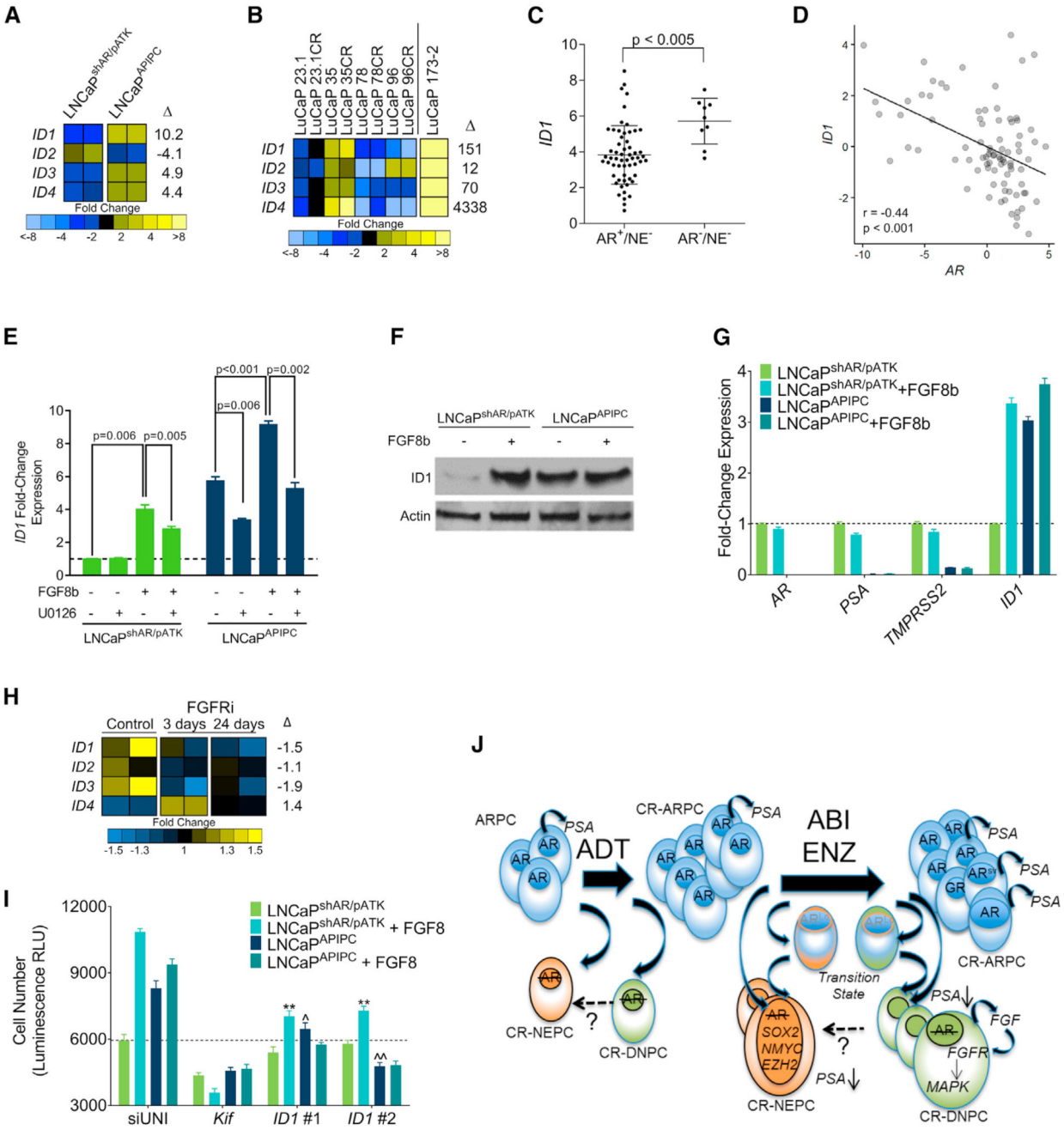

Figure 7. FGF8 Induces ID1 Expression and Castration-Resistant Growth via MAPK Pathway Activation

(A) Transcript levels of *ID1-4* in LNCaP$^{shAR/pATK}$ and LNCaP^{APIPC} cells determined by RNA-seq in two independent cultures. Fold differences of gene expression levels between LNCaPshAR/pATK and LNCaPAPIPC cells are shown.

(B) Expression of *ID1-4* in AR-positive castration-sensitive and castration-resistant (CR) PDX models (LuCaP23.1, LuCaP35, LuCaP78, and LuCaP96) and the AR-null, NE-null LuCaP173.2 PDX line. Measurements were derived from RNA-seq (n = one tumor from each LuCaP line). Fold differences of gene expression between AR-positive and AR-negative groups are shown.

(C) Transcript levels of *ID1* in AR^+/NE^- and AR^-/NE^- CRPC metastases determined by RNA-seq transcript quantitation. Log^2 counts per million (CPM) mapped reads with mean ± SD are plotted. Groups were compared by unpaired, two-tailed t test (AR^+/NE^-, n = 58 tumors from 35 men; AR^-/NE^-, n = 9 tumors from 5 men).

(D) Association of *ID1* and *AR* transcripts in CRPC metastases. Each data point represents an individual metastasis (n = 85 tumors from 50 men). Transcript levels were quantitated by RNA-seq. Pearson's correlation coefficient $r = -0.39$; $p < 0.001$.

(E) *ID1* transcripts quantitated by qRT-PCR in $LNCaP^{shAR/pATK}$ and $LNCaP^{APIPC}$ treated with 25 ng/mL FGF8 or vehicle and the MEK inhibitor U0126 or vehicle. qRT-PCR values were normalized to RPL13a expression, and compared with unstimulated $LNCaP^{shAR/pATK}$.

(F) Immunoblot of cell lysates collected from $LNCaP^{shAR/pATK}$ and $LNCaP^{APIPC}$ treated with 25 ng/mL FGF8 or vehicle probed with anti-ID1 antibody.

(G) $LNCaP^{shAR/pATK}$ and $LNCaP^{APIPC}$ were cultured under androgen-depleted conditions and treated with vehicle (PBS) or 25 ng/mL FGF8. *ID1, AR, PSA*, and *TMPRSS2* transcripts were quantitated by qRT-PCR, normalized to *RPL13a* expression, and compared with unstimulated $LNCaP^{shAR/pATK}$.

(H) Quantitation of *ID1-4* in LuCaP173.2 tumors treated with vehicle or CH-5183284 sampled 3 days or 24 days after the initiation of treatment. Transcripts were quantitated by RNA-seq of two independent tumors.

(I) $LNCaP^{shAR/pATK}$ and $LNCaP^{APIPC}$ were cultured in androgen-depleted medium and transfected with siRNA specific for target genes. Cells were treated with 25 ng/mL FGF8 or vehicle. siUNI, non-targeting control siRNA; Kif11, equimolar mixture of three siRNAs targeting Kif11 and a positive control for transfection efficiency; ID1 #1 and ID1 #2 are siRNAs targeting ID1. Relative cellular number was measured with the Cell Titer Glo luminescence assay.

(J) Schematic depicting the cellular differentiation states and underlying molecular drivers of cell survival and growth following AR pathway-directed therapy.

ADT, androgen deprivation therapy; ABI, abiraterone; ENZ, enzalutamide; CR-ARPC, castration-resistant AR program active PC; CR-NEPC, castration-resistant NE program active PC; CR-DNPC, castration-resistant PC without AR or NE program activity.

For (E), (G), and (I), significance was determined by Student's t test and data are presented as mean ± SEM (n = 3–5 replicates per data point). See also Figure S7.

KEY RESOURCES TABLE

REAGENT or RESOURCE	SOURCE	IDENTIFIER
Antibodies		
Anti-AKT	Cell Signaling	Cat# 9272, RRID:AB_329827
Ant-Phospho-Akt (Ser473)	Cell Signaling	Cat# 4058, RRID:AB_331168
Anti-AR (N-20) antibody	Santa Cruz	Cat# sc-816, RRID:AB_1563391
Anti-Anti-MAP Kinase (ERK-1, ERK-2)	Sigma	Cat# M5670, RRID:AB_477216
Anti-Anti-MAP Kinase, Activated (Diphosphorylated ERK-1/2)	Sigma	Cat# M9692, RRID:AB_260729
Anti-FGF8 MAb	R&D Systems	Cat# MAB323, RRID:AB_2102956
Anti-Id1	Biocheck Inc.	Cat# 195-14; RRID: AB_115761
Anti-Anti-MAP Kinase (MEK 1/2)	Sigma	Cat# M5795, RRID:AB_260593
Anti-phospho-MEK1 (Ser298)	Millipore	Cat# 07-339, RRID:AB_310533
Anti-Prostate Specific Antigen	Dako	Cat# M0750, RRID:AB_2281105
Anti-Actin	Santa Cruz	Cat# sc-1616, RRID:AB_630836
Anti-Chromogranin A	Dako	Cat# M0869, RRID:AB_2081135
Anti-Synaptophysin	Dako	Cat# M0776, RRID:AB_2199013
Anti-Androgen Receptor	BioGenex	Cat# MU256-UC
Anti-Human Cytokeratin	Dako	Cat# M351501-2, RRID:AB_2631307
Anti-Synaptophysin	Santa Cruz	Cat# sc-17750, RRID:AB_628311
Biological Samples		
Patient-derived xenografts	University of Washington	LuCaP
Human localized and metastatic tumors	University of Washington Prostate Cancer Donor Autopsy Program	
Chemicals, Peptides, and Recombinant Proteins		
Power SYBR Green PCR Master Mix	ThermoFisher	Cat#4367659
DNeasy Blood & Tissue Kit	Qiagen	Cat#69506
Matrigel Matrix Growth Factor Reduced	BD Biosciences	Cat#354230
Teklad laboratory animal diets (doxycycline)	Envigo	Cat#td.04104
PD 173074	R & D Systems	Cat#3044/50
Ganciclovir	inVIVOgen	Cat#sud-gcv

REAGENT or RESOURCE	SOURCE	IDENTIFIER
MDV3100	Medivation Inc.	N/A
Recombinant Human/Mouse FGF-8b	R & D Systems	Cat#423-F8-025
Pierce Phosphatase Inhibitor Mini Tablets	ThermoFisher	Cat#88667
Pierce Protease Inhibitor Mini Tablets	ThermoFisher	Cat#88665
Goat anti-Rabbit IgG (H+L) Secondary Antibody	ThermoFisher	Cat#31460
Goat anti-Mouse IgG (H+L) Secondary Antibody	ThermoFisher	Cat#31430
SuperSignal West Pico Chemiluminescent Substrate	ThermoFisher	Cat#34087
Methyltrienolone (R1881)	Perkin Elmer	Cat#NLP005005mg
U0126	Cell Signaling Technology	Cat#9903
ESP3I	ThermoFisher	Cat#ER0451
RNeasy Plus Micro Kit	Qiagen	Cat#74034
TruSeq RNA Library Preparation Kit v2	Illumina	Cat#RS-122-2001
TruSeq Stranded mRNA Library Preparation Kit	Illumina	Cat# RS-122-2101
gentleMACS M Tubes	Miltenyi Biotec	Cat# 130-096-335
RNA STAT-60	Tel-Test	Cat# Cs-502
Critical Commercial Assays		
CultreCoat Low BME Cell Invasion Assay, 96 well	R & D Systems	Cat#3481-096-K
CyQUANT Cell Proliferation Assay Kit	ThermoFisher	Cat#C7026
CellTiter-Glo Luminescent Cell Viability Assay	Promega	Cat#G7570
ApoLive Glo	Promega	Cat#G6411
Deposited Data		
Raw and analyzed Expression Microarray	Kumar et al., 2016	GEO: GSE77930
Raw and analyzed aCGH Microarray Data	Kumar et al., 2016	GEO: GSE77930
Expression microarray, aCGH Copy Number and Exome Sequencing Mutations MAF Data – FHCRC/ UW cohort	Kumar et al., 2016	http://www.cbioportal.org/study?id=prad_fhcrc
Analyzed RNAseq data – SU2C cohort	Robinson et al., 2015	http://www.cbioportal.org/study?id=prad_su2c_2015
RNAseq data	This study	GEO: GSE99381
Experimental Models: Cell Lines		
LNCaP	ATCC	ATCC CRL-1740
LNCaP^{shAR}	Laboratory of P.S. Rennie	Cheng et al., 2006

REAGENT or RESOURCE	SOURCE	IDENTIFIER
shAR/pATK		
LNCaP	This Study	N/A
LNCaP^{APIPC}	This Study	N/A
PacMetUT1	Laboratory of D.A. Troyer	Troyer et al., 2008
PacMet AR-null #1, #2	This Study	N/A
22RV1	ATCC	CRL-2505
NCI-H660	ATCC	CRL-5813
Experimental Models: Organisms/Strains		
NOD-*scid* IL2Rgamma^{null}	The Jackson Laboratory	005557
CB-17 SCID	Charles River	236
Oligonucleotides		
esiRNA targeting human *KIF11* CAUUGACAGUGGCCGAUAA	Sigma	Cat#SASI_Hs01_00161689
esiRNA targeting human *KIF11* CUGUACUACAGGAAUUGAU	Sigma	Cat#SASI_Hs01_00161696
esiRNA targeting human *KIF11* CAACAAGGAUGAAGUCUAU	Sigma	Cat#SASI_Hs01_00161697
esiRNA targeting human *ID1* CCUCUCUGCACACCUACUA	Sigma	Cat#SASI_Hs01_00057899
esiRNA targeting human *ID1* GGGCGCUCCUCUCUGCACA	Sigma	Cat#SASI_Hs01_00246329
siRNA Targeting Human *FGF8* #1 CAAGAGCAACGGCAAAGGCAA	Qiagen	Cat#SI00145600
siRNA Targeting Human *FGF8* #2 GCGCUUCGAGUUCCUCAACUA	Qiagen	Cat#SI02636725
siRNA Targeting Human *FGF9* #1 UUGGAUAUACCUCGCCUAAUA	Qiagen	Cat#SI00031332
siRNA Targeting Human *FGF9* #2 CAGAGUCGGUUAGAGAGUAAA	Qiagen	Cat#SI04932011
sgRNA protospacer CTCCGGACCTTACGGGGACATG	This Paper	N/A
*AR*_Exon1_sgRNA+ caccgCTCCGGACCTTACGGGGACATG	This Paper	N/A
*AR*_Exon1_sgRNA-aaacCATGTCCCCGTAAGGTCCGGAGc	This Paper	N/A
AR-fwd CRISPR verification primer CGACTTCACCGCACCTGATG	This Paper	N/A
AR-rev CRISPR verification primer AGGGCACGCAGCAGAAATTAG	This Paper	N/A
qRT-PCR Primers	This Paper	Table S1
Recombinant DNA		
HSV1-tk gene in pORF vector	inVIVOgen	Cat#porf-hsv1tk
pATK	This paper	N/A

REAGENT or RESOURCE	SOURCE	IDENTIFIER
lentiCRISPRv2	Sanjana et al., 2014	Addgene Plasmid #52961
Software and Algorithms		
Prism v7	GraphPad	https://www.graphpad.com/scientific-software/prism/
TopHat v2.1.0	Kim et al., 2013	https://ccb.jhu.edu/software/tophat/index.shtml
Genomic Alignments v1.0.1	Lawrence et al., 2013	https://bioconductor.org/packages/release/bioc/html/GenomicAlignments.html
edgeR v3.16.5	Robinson et al., 2010	https://bioconductor.org/packages/release/bioc/html/edgeR.html
Ape v4.1	Paradis et al., 2004	https://cran.r-project.org/web/packages/ape/index.html
GSVA v1.24.0	Hänzelmann et al., 2013	https://bioconductor.org/packages/release/bioc/html/GSVA.html
Scatterplot3d v0.3–40	Ligges and Machler, 2003	https://cran.r-project.org/web/packages/scatterplot3d/index.html
GSEA v2.2.4	Subramanian et al., 2005	http://software.broadinstitute.org/gsea/index.jsp
MSigDB v6.0	Subramanian et al., 2005	http://software.broadinstitute.org/gsea/msigdb
Other		
RNAiMax lipofectamine	ThermoFisher	Cat#13778030
Lipofectamine 2000	ThermoFisher	Cat#11668019
FBS Charcoal Dextran Stripped	Gemini Bio-Products	Cat#100–119